Univerza v Ljubljani
Fakulteta za računalništvo in informatiko

Žiga Zupanec

Ocenjevanje trajektorije primikajoče tarče z merjenjem razdalj v UWB

magistrsko delo

magistrski program druge stopnje
računalništvo in informatika

Ljubljana, 2016

Univerza v Ljubljani
Fakulteta za računalništvo in informatiko

Žiga Zupanec

Ocenjevanje trajektorije primikajoče tarče z merjenjem razdalj v UWB

magistrsko delo

magistrski program druge stopnje
računalništvo in informatika

Mentor: doc. dr. Luka Šajn
Somentor: izr. prof. dr. Fabio Ricciato

Ljubljana, 2016

University of Ljubljana
Faculty of Computer and Information Science

Žiga Zupanec

Trajectory estimation of a moving target from UWB ranging measurements

masters thesis

the 2nd cycle masters study programme
computer and information science

Supervisor: Luka Šajn, PhD Asst. Prof.
Co-supervisor: Fabio Ricciato, PhD Assoc. Prof.

Ljubljana, 2016

Declaration of Masters Thesis authorship

I, the undersigned Žiga Zupanec am the author of the Master Thesis entitled:

Trajectory estimation of a moving target from UWB ranging measurements

With my signature, I declare that:

- the submitted Thesis is my own unaided work under the supervision of Luka Šajn, PhD Asst. Prof. and co-supervision of Fabio Ricciato, PhD Assoc. Prof.,
- all electronic forms of the Masters Thesis, title (Slovenian, English), abstract (Slovenian, English) and keywords (Slovenian, English) are identical to the printed form of the Masters Thesis,
- I agree with the publication of the electronic form of the Masters Thesis in the collection "Dela FRI".

In Ljubljana, 22nd of March 2016 Author's signature:

Acknowledgments

I would like to thank my supervisors, Asst. Prof. Luka Šajn and Assoc. Prof. Fabio Ricciato for all their time, useful comments and guidance during the making of this thesis. Furthermore I would like to thank my parents and my brother for their support along the way. I would like to thank my cousins who helped me during the experiments. Finally, I would like to thank Multilux for providing LIPS equipment and especially Denis and Grega for all their help.

Žiga Zupanec, 2016

Contents

Abbreviations

BT Bluetooth. 2

CDF Cumulative distribution function. 9, 10, 17, 18, 21, 27, 35, 38, 50, 55, 63–66

FMUg `fminunc` with user-supplied gradient. 7, 17, 18, 63–66

GPS Global Positioning System. 1

GT Ground truth. 8, 9, 11, 17, 20, 27, 28, 31, 32, 34, 47, 50–52

IPS Indoor positioning system. 1

ISM Industrial, scientific and medical radio band. 4

IV Intravenous. 42, 43, 81

LIPS Local indoor positioning system. 2, 4, 5, 23, 24, 57

NLOS Non-line-of-sight. iii, 8, 9, 11

NLS Non-linear least squares. iii, 6

RFID Radio-frequency identification. 2

RMS root mean square. 19, 21, 35, 39, 50, 56

RSS Received Signal Strength. 2

TOF Time of flight. 4

USB Universal Serial Bus. 6

UWB Ultra-wideband. iii, 2

WLAN Wireless local area network. 2, 58

Povzetek

V tem magistrskem delu rekonstruiramo začetno pozicijo ter hitrost in smer premikajoče se tarče v realnem okolju. Predlagamo postopek, ki ta dva vektorja izračuna na podlagi ocenjenih razdalj med premikajočo se tarčo in skupkom stacionarnih oddajnikov. Bistvo postopka je optimizacija kriterijske funkcije z metodo najmanjših kvadratov. Opravili smo obsežne eksperimente tako na prostem, kot v zaprtem prostoru. Podrobno smo analizirali dobljene rezultate in jih pokomentirali. Pri eksperimentih na prostem je napaka med končnim mestom trajektorij in dejansko lokacijo tarče manjša od enega metra pri razdalji 16 m. V zaprtem prostoru smo rahlo izboljšali natančnost obstoječega komercialnega sistema za določanje lokacije.

Ključne besede

Merjenje razdalj, metoda najmanjših kvadratov, odsotnost iz neposredno vidnega polja, izven, ultra širok frekvenčni pas, premikajoča se tarča, lokacijska napaka, mobilna tarča, ocenjevanje hitrosti

Abstract

In this master thesis we reconstruct position and movement of a blind target node in a realistic environment based on ranging measurements from a set of fixed anchor nodes. We propose a method for trajectory estimation of a moving node based on minimizing residual sum defined as the difference between a reported and the actual distance from the anchor nodes. We devised extensive and complex outdoor as well as indoor experiments with exploratory data analysis and interpretation of the results. Our findings show that the method achieves sub one metre accuracy at 16 m distance in an outdoor environment and a slight improvement over existing point based localization system in an indoor environment.

Keywords

Ranging measurements, Non-linear least squares (NLS), Non-line-of-sight (NLOS), Ultra-wideband (UWB), blind node, localization error, mobile node, target node, velocity estimation

Razširjeni povzetek

Potreba po uporabi sistema za določanje lokacije v zaprtih prostorih nastaja pri avtomatizaciji določenih opravil (skladiščenje izdelkov), nadzora ljudi in blaga (trgovinski centri), reševanje pri nesrečah (rudniki), ipd. Delovanje sistema za določanje lokacije v zaprtih prostorih lahko analogno ponazorimo z delovanjem globalnega sistema pozicioniranja (GPS). GPS sateliti po analogiji ustrezajo stacionarnim oddajnikom. To so t.i. »sidra«. Sidra so postavljena visoko, praviloma na strop, in se ne premikajo. Njihova pozicija v zamišljenem koordinatnem sistemu je znana. Premikajoča tarča pa je opremljena s sprejemnikom, ki ves čas ocenjuje razdaljo med sabo in okoliškimi sidri (po analogiji GPS sprejemnik). Za določitev pozicije v dvo-razsežnem okolju (2D) potrebujemo najmanj tri sidra. Če želimo oceniti še višino tarče, potrebujemo meritve štirih ali več sider.

V eksperimentih uporabljamo že razvito in celovito rešitev LIPS podjetja Multilux d.o.o. Sistem LIPS deluje v frekvenčnem območju 2.45 GHz — industrijskem, znanstvenem in medicinskem radijskem spektru. Naš cilj je bil nadgraditi njihov že obstoječ točkovni pozicijski sistem s postopkom, ki lokacijo premikajoče tarče določi na podlagi njene trajektorije. V ta namen smo prilagodili postopek za ocenjevanje trajektorije z merjenjem moči signala (angl. RSS) [1, 2]. Namesto moči signala uporabljamo meritve oddaljenosti med tarčo in sidri, ki so bolj zanesljive. Meritve oddaljenosti so tudi najbolj »surovi podatki« do katerih lahko dostopamo, ne da bi za to bilo treba poseči v sistem. Razvit postopek je zmožen obdelati meritve z napakami, ki nastanejo pri procesiranju podatkov med napravami. Postopek je odporen,

tudi ko je med tarčo in določenim sidrom več hkratnih poti signalov, dokler prevladuje neposredna pot signala. Za primere, kjer so prevladujoče posredne poti signalov ali pa neposredna pot med tarčo in sidrom ne obstaja, smo uporabili tri hevristične metode:

- **peti percentil meritev**; ta metoda je uporabna samo za postanke, tj. situacije, v katerih je tarča v mirovanju. V obdobju mirovanja zajamemo določeno število meritev (oddaljenost med tarčo in sidrom), ki jih opišemo s porazdelitveno funkcijo. Odčitano vrednost pri petem percentilu za vsako sidro uporabimo kot vhod v postopek za ocenjevanje trajektorije, ki nam vrne ocenjeno lokacijo. Ideja »petega percentila« je, da se na čisto spodnjem koncu porazdelitvene funkcije ognemo meritvam z negativno napako, hkrati pa odrežemo zajeten del, kjer je pričakovan izvor napake posredna pot signala.

- **robustna srednja vrednost trojk**; pri tej metodi se zanašamo na pravilno ocenjeno meritev večine. Izmed množice vseh sider naredimo vse možne kombinacije treh. Meritve ene trojke predstavimo kot množico možnih lokacij za določeno časovno obdobje. Izmed točk vseh trojk ustvarimo novo, navidezno točko, ki predstavlja aritmetično sredino (centroid) gruče. Nato iz gruče odstranimo 1 % vseh točk, ki so najbolj oddaljene od centroida, in na preostali množici točk določimo nov centroid. Ta postopek iterativno ponavljamo, dokler ne ostane le še 50 % prvotnih točk. Med temi zopet določimo centroid, ki je končni rezultat metode.

- **odstranjevanje največje napake**; tu gre za ponavljanje postopka, ki določi lokacijo premikajoče tarče, dokler ne zadostimo določenim pogojem. Po začetni aplikaciji postopka dobimo dva vektorja, začetno pozicijo in hitrost, vsakega s po tremi komponentami. Spomnimo, da postopek določanja lokacije temelji na vsoti kvadratov najmanjše napake. Vse kvadrirane člene vsote uredimo po velikosti in izločimo 0.5 % meritev z največjo napako. Postopek ponavljamo toliko časa, da

obdržimo 80 % do 90 % začetnih meritev.

Opisan postopek za oceno trajektorije smo preverili z računalniško simulacijo v programskem paketu MATLAB. Rezultati so bili v skladu s pričakovanji, kar je potrdilo pravilno implementacijo postopka.

Izvedli smo uvajalne eksperimente na prostem. Na ravni travniški površini smo kosilnico premikali premočrtno in s konstantno hitrostjo med sidri postavljenimi na krožnici s polmerom osmih metrov. Napaka med ocenjenim končnim postankom in dejanskim končnim postankom je bila vedno manjša od enega metra. Glavni del naloge je bil testiranje metod v zaprtem prostoru. Eksperimente smo izvedli v jedilnici Fakultete za računalništvo in informatiko v času, ko je bila jedilnica prazna. Jedilnico smo izbrali, ker je prostorna in ima visoke strope, kar je zaželen pogoj pri uporabi sistema LIPS. Izvedli smo šest kompleksnih eksperimentov z različnimi obhodi in pri različnih hitrostih sicer enakomernega gibanja. Dobljeni rezultati so bili zaradi slabe kakovosti zajetih podatkov vidno slabši od rezultatov dobljenih na prostem. Slabšo kakovost podatkov gre pripisati številčnejšim odbojem signalov, slabši pokritosti prostora s sidri na določenih mestih, bližini sten in elektromagnetnim motnjam.

Chapter 1

Introduction

An Indoor positioning system (IPS) is a system that determines the position (location) and/or movement of an object within a confined space. The system consists of a set of fixed, static nodes called anchors and an undetermined position of a blind node roaming freely within the confined space. Perhaps the most widely known positioning system is the Global Positioning System (GPS) [3]. This system employs a network of earth orbiting satellites and terrestrial GPS receivers. Each GPS receiver determines its location based on data received from the satellites [4]. If we draw a parallel to the Global Positioning System, the anchor nodes of the IPS resemble satellites and the blind node resembles a GPS receiver device. Anchor nodes, a blind node and a processing unit are integral parts of IPS.

There are cases where one cannot use GPS since it relies on direct satellite signal reception [5]. For instance, indoor environments, such as warehouses and shopping malls, underground facilities, such as basements, tunnels, underground mines, etc. One can also consider our solution as a replacement for GPS where power consumption is of concern. Yet another case of usage are devices that are not equipped with a GPS receiver or have the GPS receiver switched off most of the time. Aforementioned situations are the reason to look closer at an indoor localization system.

A multitude of technologies is suitable for obtaining an indoor position.

These technologies include and are not limited to Wireless local area network (WLAN) [1, 2, 6], Radio-frequency identification (RFID) [7], cellular-based [8], UWB [9], Bluetooth (BT) [10] and others. Liu et al. published a research of various commercially available wireless-based indoor positioning systems and solutions, which suggests that the most widely used technology uses WLAN's Received Signal Strength (RSS) to determine the target's position [11].

A common practice of determining the position of a moving target is to condense the information into one single point of location. This method yields successive points of position along the path of a target's movement. Because of various errors affecting the point based localization the tracking path is often non-linear and does not reflect the actual movement of the target [2].

Our intention is to improve positioning accuracy of a blind node by enhancing Multilux's Local indoor positioning system (LIPS) — point based positioning — system with trajectory estimation of a linearly moving node. Multilux Ltd. is a Slovenian company that develops indoor positioning systems.

Detailed problem formulation and derived resolution routine are explained in Chapter 2. We evaluate the resolution routine in a simulation scenario presented in Chapter 3. Chapter 4 describes outdoor experiments in detail. We provide extensive analysis of the gathered data along with the results of our trajectory estimation. In Chapter 5 similar experiments are conducted in an indoor environment (the faculty cafeteria). We conclude our study analysis by pointing out our observations and findings.

Chapter 2

Problem statement

The key elements to solving any problem are determining its domain and testing possible solutions. The domain in this study is the physical environment in which the system is set up. Within this environment possible solutions are tested and analyzed. This chapter describes the basic domain, formulates the problem and discusses the solutions used to reduce the impact of errors.

2.1 Scenario

Imagine a moving object within a room bound by four walls (Fig. 2.1). The object lies somewhere in the room with the initial position $\boldsymbol{P}$ and is moving towards a wall with a constant velocity $\boldsymbol{v}$. To determine the object's current position we multiply its velocity $\boldsymbol{v}$ by elapsed time t and add the result to the object's initial position $\boldsymbol{P_t} = \boldsymbol{P} + \boldsymbol{v}t$. The moving object is called a (moving) blind node because its properties are a priori unknown.

We can determine the blind node's properties by using ranging measurements (reported by the blind node) obtained from pinging anchor nodes. Anchor nodes are an integral part of the model. Their position is fixed and known to the outside observer. Ranging measurement is the distance between a blind node and an anchor. It is the path of a signal travelling from

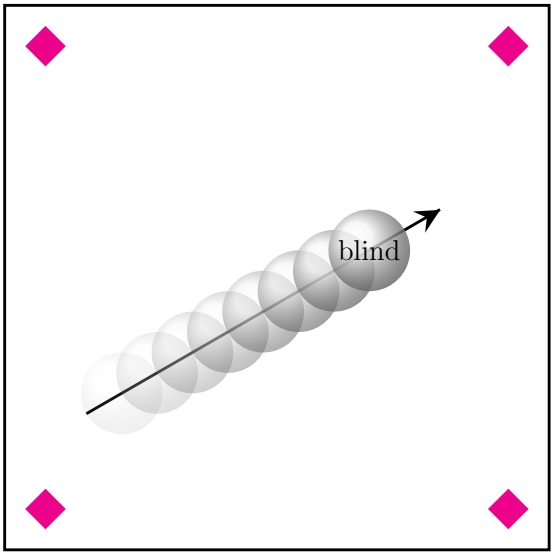

Figure 2.1: Reference scenario showing a moving blind node surrounded by four anchors.

one end to another. Signal velocity v_s is the speed at which the signal wave carries data: $v_s = \frac{c}{\sqrt{\varepsilon_r}}$, where c is the speed of light in a vacuum and ε_r is the relative dielectric constant of the air. Knowing the signal velocity and Time of flight (TOF), $\hat{\tau}$, which is the time a signal needs to travel from a transmitter to a receiver measured by a common time reference [12], signal path is computed as follows: $d = v_s\hat{\tau}$.

To obtain the blind node's trajectory in 2D space we need ranging measurements from at least three non-collinear anchors and four non-collinear anchors to get the blind node's trajectory in 3D space.

2.2 Technology

All necessary hardware used in our experiments was provided by Multilux Ltd[1]. Their proprietary point based positioning solution is called LIPS. LIPS communication devices function at the 2.45 GHz frequencies, which belong to the designated Industrial, scientific and medical radio band (ISM) [13]. The

[1]http://multilux.eu

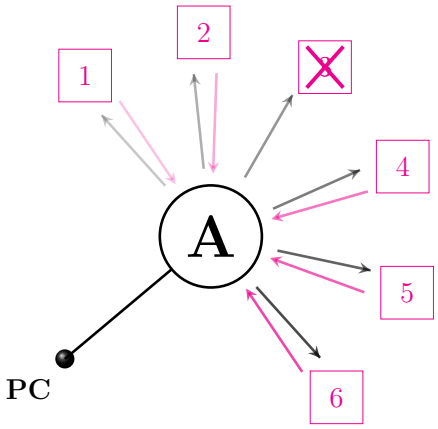

Figure 2.2: Abstract scheme of a blind node 'A' performing ranging measurements from anchor nodes (magenta color).

devices operate at very low energy levels. LIPS devices use ranging sensors developed by Nanotron Technologies. A blind node pings anchor nodes in a round-robin fashion performing two way ranging measurements (Fig. 2.2). Nanotron Technologies has developed a time of flight method that employs a ranging signal sent by a reader and an acknowledgment sent back from the tag to cancel out the requirements for clock synchronization [14]. Ranging measurement is the distance between the blind node and an anchor. The blind node periodically sends data to a processing unit that determines its position and trajectory.

Provided ranging information is as close to the "raw data" as we could get without accessing the physical layer or the device's firmware (which we have no control of). Having been able to access internal variables ($\hat{\tau}$) and modify the devices to support its broadcasting mode, we could have employed the differential time-difference of arrival (DTDoA) approach that would give us more data from all nearby devices [6]. Working with (only) ranging data posed a constraint that was considered in problem formulation.

A blind node creates a measurement packet every 130 ms or about eight times per second. A packet contains a relative timestamp, reflecting time of its formation and an n-tuple with ranging information, where n is the

Table 2.1: Example of a measurement packet.

timestamp	anchor ID	ranging	status
1452967702506	1	21.49	OK
1452967702506	2	12.64	OK
1452967702506	3	0.00	ERR
1452967702506	4	2.80	OK
1452967702506	5	13.51	OK
1452967702506	6	11.29	OK

number of anchor nodes deployed in a given scenario (Table 2.1). Ranging information is a distance/status pair for i-th anchor node. A stream of packets is then sent to the processing unit via serial-over-Universal Serial Bus (USB) connection. The processing unit utilizes NLS formula to estimate the blind node's trajectory.

2.3 Problem formulation

Trajectory estimation is a non-linear least squares problem defined as a set of given ranging measurements over a period of time to determine the blind node's initial position $\boldsymbol{P} = [x, y, z]^\intercal$ and its velocity $\boldsymbol{v} = [v_x, v_y, v_z]^\intercal$.

With an array of ranging measurements $\boldsymbol{D}$ recorded for the duration of a single walk (one linear trajectory), the problem can be expressed as an NLS optimization function:

$$[\hat{\boldsymbol{P}}_{\boldsymbol{0}}, \hat{\boldsymbol{v}}] = \arg\min_{\boldsymbol{P},\boldsymbol{v}} \sum_{k=1}^{K} \sum_{m \in \boldsymbol{D_k}} \left(\|\boldsymbol{P} + \boldsymbol{v}t_m - \boldsymbol{P_k}\| - d_{k,m} \right)^2, \tag{2.1}$$

where

- $\boldsymbol{P}$ is the initial position of the blind node;
- $\boldsymbol{v}$ is the velocity vector of the blind node;

- K is the number of deployed anchors;
- $\boldsymbol{D_k}$ is an array of recorded measurements for k-th anchor;
- t_m is the relative time of m-th measurement starting from $t_0 = 0$;
- $\boldsymbol{P_k}$ is the position of k-th anchor;
- $d_{k,m}$ is the distance between the blind node and k-th anchor taken from m-th measurement.

This function computes such $\boldsymbol{P_0}$ and $\boldsymbol{v}$ where the squared difference between the measured distance $d_{k,m}$ and the computed distance based on time $\|\boldsymbol{P} + \boldsymbol{v}t_m\|$ to all the anchors is minimal. The solution to this problem can be solved with MATLAB's unconstrained solver `fminunc`. The solver uses a Quasi-Newton method to find the local minimum. To speed up the process, we resort to `fminunc` with user-supplied gradient (FMUg). The described routine can be used in MATLAB as:

Code 1 The use of `fminunc` in MATLAB.

```
1: x0 = [0, 0, 0, 0, 0, 0];
2: % Initial guess [x_0, y_0, z_0, v_x, v_y, v_z].
3:
4: fun = @(y)objfun_gradient(y, anchor_positions, D);
5: % Gradient of the objective function with additional parameters.
6:
7: options = optimoptions(@fminunc, 'SpecifyObjectiveGradient', true, 'Algorithm', '
       quasi-newton');
8: % Tell fminunc to use cutom gradient and Quasi-Newton method.
9:
10: [traj_est, fval] = fminunc(fun, x0, options);
11: % Solve NLS.
```

The Least Squares solution represents the Maximum Likelihood estimate for Gaussian errors with zero mean [1, 2]. This error is caused by delays in data processing between communication devices. If an error is strictly

positive, the cause is attributed to a NLOS between the node and an anchor (heavy multipath error). In order to handle these errors, we developed several heuristic methods that work in conjunction with our resolution routine.

2.4 Error model

In practical experiments the measured distance is not equal to the Ground truth (GT) distance due to various elements. We analyzed two types of physical errors:

- small, symmetric distance error (sources are hardware delays and multipath)
- large, positive distance error (source is NLOS with heavy multipath).

Multipath is a phenomenon where the signal path between a receiver and a transmitter comes from direct and multiple indirect sources (Fig. 2.3). Multipath error depends on amplitude, phase and on the received signal itself [15]. In line of sight (LOS) conditions, the strongest path of the signal typically corresponds to the first path, while in NLOS conditions weak components typically precede the strongest path [16]. Cases where there is no direct signal and cases where indirect signals are predominant are labelled heavy multipath. Heavy multipath is particularly present in indoor environments. There are no formal methods for detecting NLOS from ranging measurements. To tackle this problem we employ three different heuristic methods.

2.5 Pruning heuristics

In order to trim the erroneous data, a number of different statistical methods was employed in the process. Simpler methods based on the arithmetic mean and the median proved to be inferior to the more sophisticated ones. As a result the three pruning heuristics described in this chapter served as our

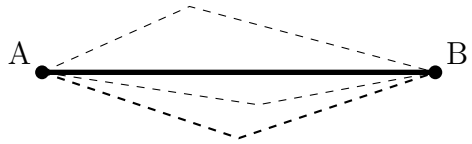

Figure 2.3: Multipath — the signal path between transmitter A and receiver B taking various routes.

filtering methods. The 5th percentile heuristic and the residual pruning method are strictly pre- and postprocessing mehtods, respectively while the robust mean method functions in both steps. Depending on the quality of the gathered data, each pruning heuristic displayed various degrees of accuracy. The preliminary research on the pruning methods showed that other studies mostly depend on the Kalman filter [17] for its simplicity. In our case, the Kalman filter is not a viable solution since it is very sensitive to outliers and large errors [2].

2.5.1 5th percentile of distances

This method was developed as a more robust method compared to the statistical median method due to the distribution of the reported distances from an anchor nodes. A limitation of this method is that it can only be applied to segments where the target node is stationary. The distance errors are obtained by subtracting measured data from the GT and used to form a Cumulative distribution function (CDF) for each anchor.

Given the properties of a physical environment, especially indoors, we anticipate a bimodal distribution of the collected data (Fig. 2.4). The 5th percentile of CDF distribution was chosen to avoid the negative distance error component between devices on the lower end and to cut off measurements with positive distance error components caused by NLOS (Fig. 2.5).

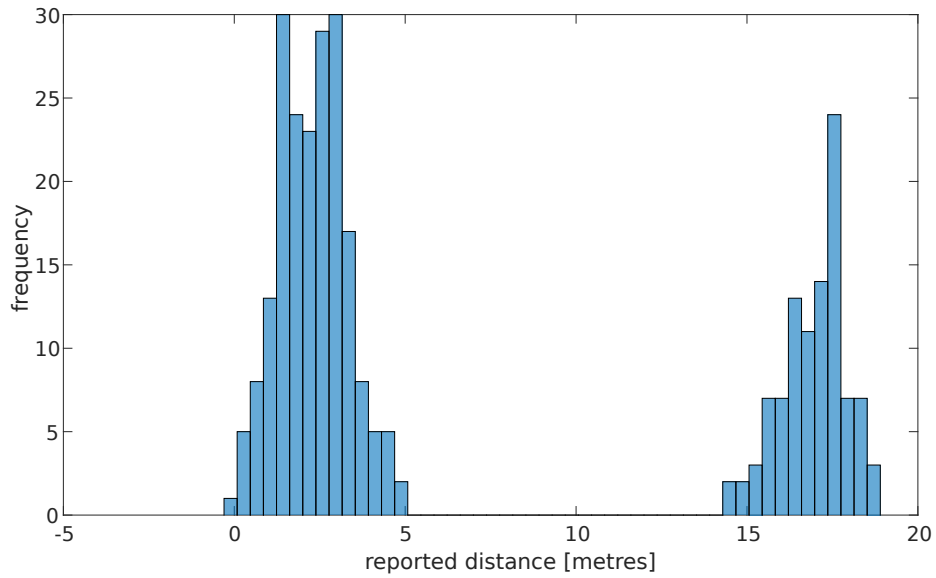

Figure 2.4: A graphical representation of the bimodal distribution.

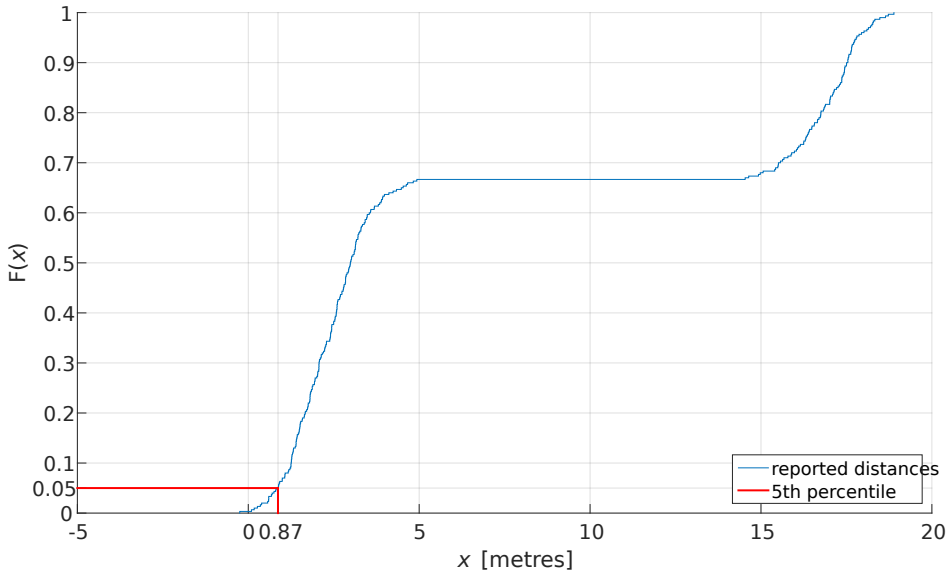

Figure 2.5: CDF plot of bimodal distribution from Figure 2.4.

2.5.2 Robust mean over n-tuple

Clustering and outlier rejection further reduce the error caused by NLOS as well as errors from other sources. This is based on the fact that the direct path signals of multiple anchor nodes will localize the blind node close to the GT location, while reflection path signal will localize the blind node at random locations [15].

For all experiments conducted in this work 3-tuple, $\binom{6}{3}$ formation was selected for the six anchors. This provided us with 20 combinations of triplets in the preprocessing step. A point based localization was then used to form a cloud of points for each triplet. In the postprocess a centroid was determined among all the points as the arithmetic mean value over all clouds. The furthest 1 % of the points was eliminated and a new centroid was elected [6]. This process was iterated until there were 50 % of the initial number of points left. A visual representation of the outcome of the described procedure is depicted in Figure 2.6.

2.5.3 Residual pruning

Residual pruning is a method that repeats the resolution routine until a stop condition is met. After its initial application, the outcome are two vectors — one is the initial position $\boldsymbol{P_0}$, the other one is velocity vector $\boldsymbol{v}$. The residuals used in the resolution routine are then unrolled, sorted and 0.5 % packet measurements (0.5 % of m from $\boldsymbol{D}$) representing the largest residuals are discarded. This process is iteratively repeated until there are 80 % to 90 % packet measurements left in $\boldsymbol{D}$. The expected outcome of this method is to give a better approximation to the GT trajectory by identifying and eliminating outliers after localization.

2.5.4 Pruning heuristics analysis

Of the three described heuristic methods only one is used for a given computation. The best performing method is determined by the quality of the

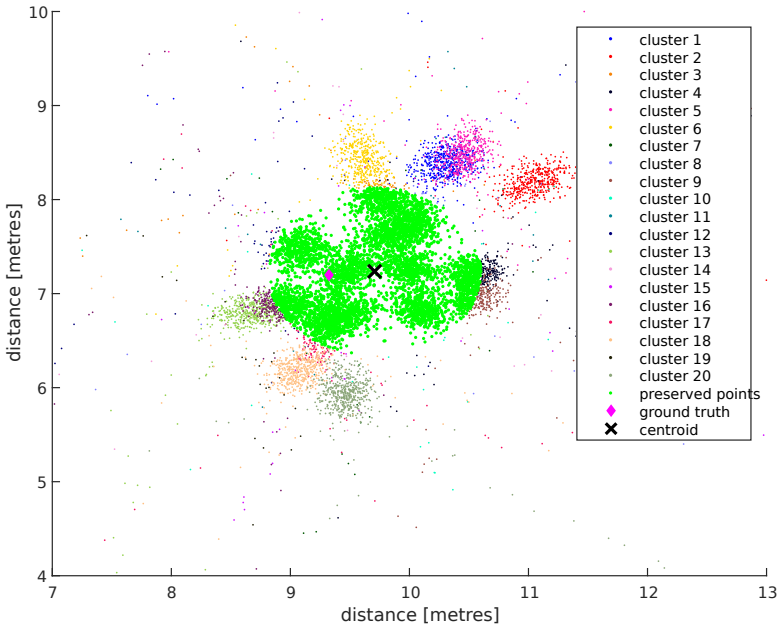

Figure 2.6: Robust mean over triplet with a 50 % retention rate (green cluster) and iteration dropout of 1 %.

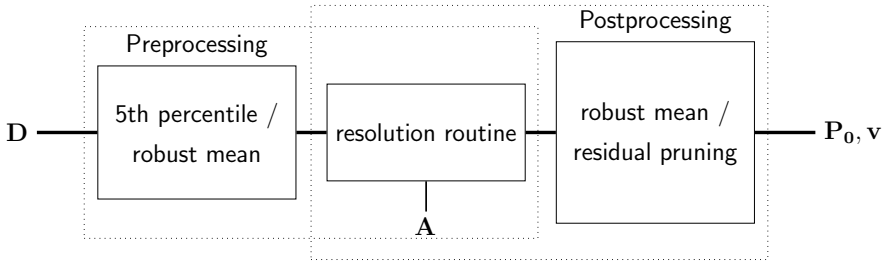

Figure 2.7: Localization pipeline.

input data which is further described in chapters 4 and 5.

Preprocessing heuristics require distance data as input. The processed distance data $\hat{\boldsymbol{D}}$ is then piped into the resolution routine together with anchors' positions $\boldsymbol{A}$ and the estimated initial position of the target node. The result of the entire pipeline is the target node's initial position $\boldsymbol{P_0}$ and its velocity $\boldsymbol{v}$. The speed of the pipeline depends on the heuristic method's properties, the most defining ones being the amount of data and the possible iterative nature of the heuristic.

Chapter 3

Preliminary simulations

Before implementing and testing an actual physical system, simulation is often a less resource intense method of obtaining preliminary results. These can then be used to improve the physical implementation of the system.

3.1 Test environment

A computer simulation was run on MATLAB with six anchors positioned on a plane in such manner that they formed a convex polygon (Fig. 3.1). The circumference measures roughly 200 m × 150 m. A convex polygon topology was selected in favour of a square one to avoid symmetry problem where more than one anchor lies in the line of sight. The height of all anchors was set at 5 m above the ground.

The blind node was positioned in the vicinity of the anchors and moved in a linear motion with a constant speed chosen uniformly at random on an interval between 0 to 4 $\mathrm{m\,s^{-1}}$. The blind node had a constant height of 1 m above the ground. The position of the anchors and the height of the blind node is known to the algorithm beforehand.

One trial consists of a randomly chosen initial blind node's position and a randomly chosen initial blind node's velocity. The blind node is then tracked for 20 frames (20 seconds), meaning that 20 distances (ranging measure-

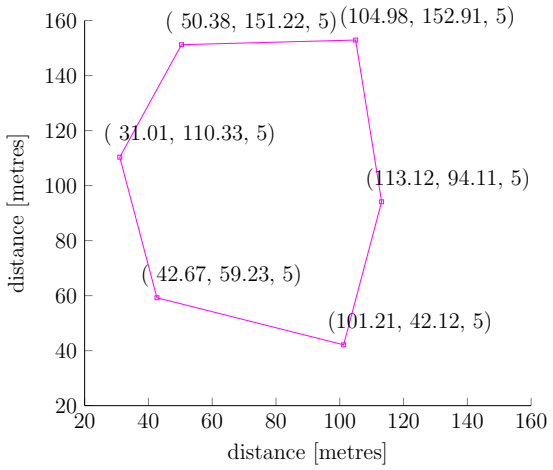

Figure 3.1: Test environment.

ments) were obtained between the blind node and each anchor.

The measured distances are randomly affected by the normal distribution with the expected value of 0 ($\mu = 0$) and the standard deviation σ of 5 metres for the first simulation (referred as Simulation A) and σ of 10 metres for the second simulation (Simulation B). The position of the anchors and the collected data is fed to the resolution routine presented in the equation (2.1).

A trajectory lies in one of the four possible areas:

- inside: completely inside the convex polygon formed by six anchors.
- inside-out: starting inside the polygon but ending outside of it.
- outside-in: starting outside the polygon but ending inside the polygon.
- outside: starting and ending outside the polygon.

Once the area is determined, the error as an Euclidean distance between two points (the ground truth point and the estimated point) for a given method is calculated. We track error for the middle and the final point of each trajectory. As the name suggests the middle (mid) point is halfway between the initial and the final point of a trajectory.

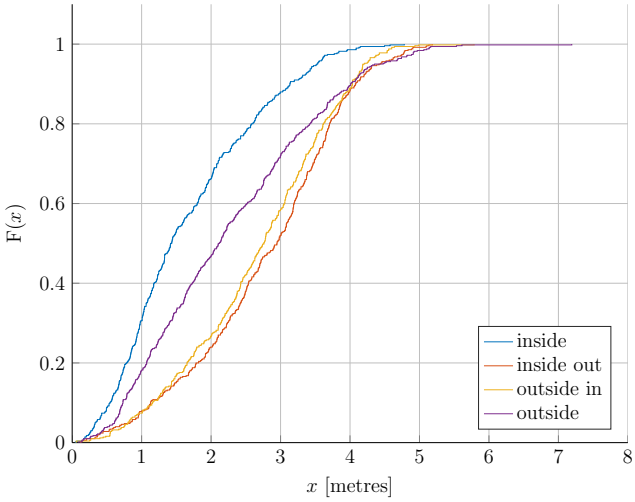

Figure 3.2: Simulation A. CDF for FMUg on mid point, $\sigma = 5$.

The described procedure is repeated until there are 500 such trials for each area case. The error is visualized as the CDF for four possible area cases, all superimposed on one figure. We focused on the mid and final points with two different standard deviations ($\sigma = 5$ and $\sigma = 10$) shown in four separated plots. (See Figures 3.2, 3.3, A.5 and A.6.) A similar pattern was observed in both, Simulation A and Simulation B.

The resolution routine yields best estimates for trajectories that lie inside the convex polygon. This is attributed to the fact that distances between the blind node and the anchors are approximately the same and the lines of sight of these anchors do not intersect with one another.

3.2 Error on mid and final points

We define the error on the mid and final point as the distance between the GT trajectory's mid and final point and the estimated mid and final point for the given resolution routine (Eq. (2.1)).

An unexpected linear correlation between the velocity modulus $\|\boldsymbol{v}\|$ and the error on mid and final point became evident. As the velocity increased,

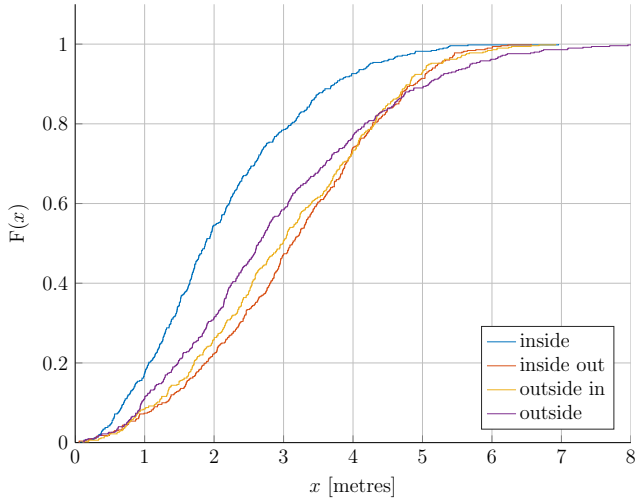

Figure 3.3: Simulation A. CDF for FMUg on final point, $\sigma = 5$.

the error increased. We observed such a trend in all trials as well as in trials using values only up to the 90th percentile and the median bottom half trials only. Figures 3.4 and 3.5 show the error linearly increases as the speed increases for all tested subsets.

There were 5000 trials for each area location. Each line had 41 markers (the velocity modulus resolution was $0.1\,\mathrm{m\,s^{-1}}$). Each marker on the line is therefore a result of 122 trials on average.

If we consider only trials with errors below the median (Fig. A.8, A.10), point error on the trajectories inside the polygon becomes almost constant. Point error on the trajectories that lie completely outside the polygon is significantly reduced as well.

This was chosen as our reference scenario. The described methodology was the used for all the following simulation scenarios.

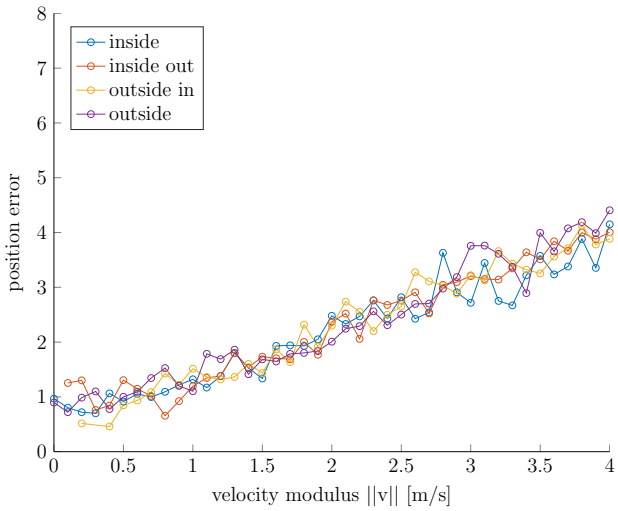

Figure 3.4: Velocity modulus vs. position error, RMS on mid point, $\sigma = 5$.

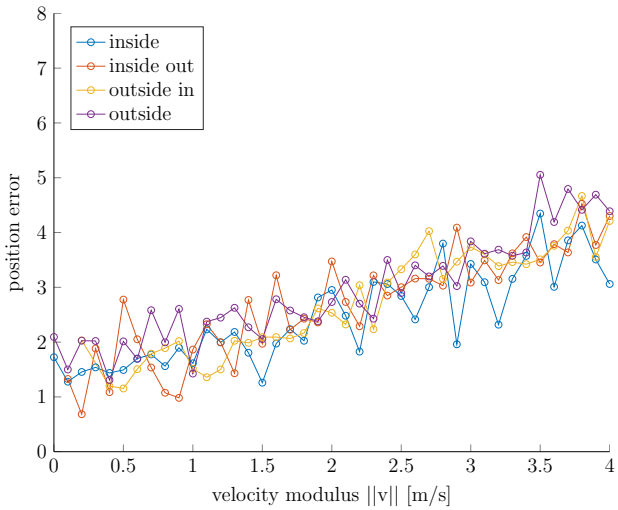

Figure 3.5: Velocity modulus vs. error, RMS on final point, $\sigma = 5$.

3.3 Adding positive error component

In the first scenario a positive error component was added, randomly chosen from a uniform distribution between 0 and $\beta\ell_r$.

$$\ell_m(x) := \begin{cases} \ell_r + r_c + r_u & ; x < \alpha, \\ \ell_r + r_c & ; x \geq \alpha. \end{cases} \tag{3.1}$$

- ℓ_r represents the GT distance from the r-th anchor to the blind node;
- α represents the threshold for the type of error added to the measured distance. Depending on a random variable x, one of two possible outputs is selected;
- β is the multiplier applied to the GT distance ℓ_r;
- r_c is a random variable from normal distribution, i.e. $r_c \sim \mathcal{N}(0, \sigma)$;
- r_u is a random variable from continuous uniform distribution, i.e. $r_u \sim$ Unif(0, $\beta\ell_r$).

We used $\alpha = 0.5$, $\beta = 0.5$ and $\sigma = 5$. We see that point error increases significantly (Figs. A.1 and A.3) over reference scenario. The relation between the velocity modulus and point error is no longer linear but constant (Figs. A.11 - A.16).

In the second scenario, we applied a positive error component randomly from the uniform distribution within the range between 0 and the fixed value F.

$$\ell_m(x) := \begin{cases} \ell_r + r_c + r_F & ; x < \alpha, \\ \ell_r + r_c & ; x \geq \alpha, \end{cases} \tag{3.2}$$

where

- ℓ_r represents the GT distance from the r-th anchor to the blind node;

- r_c is a random variable from the normal distribution, i.e. $r_c \sim \mathcal{N}(0, \sigma)$;
- r_F is a random variable from the continuous uniform distribution, i.e. $r_F \sim \text{Unif}(0,\, F)$.

We used $\alpha = 0.5$, $\beta = 0.5$, $\sigma = 5$ and $F = 10$. Point errors on mid and final points increased slightly compared to our reference scenario. Looking at final point errors we see that the velocity modulus no longer affected position errors. The position errors are constant regardless of the velocity modulus. See the rest of CDF figures and RMS vs. velocity modulus results of various error components in the Appendix A.

Chapter 4

Outdoor experiments

These experiments offer an ideal physical environment in which the system was set up. While it is next to impossible to have such an ideal environment in a practical implementation, the results of these experiments showcase the effectiveness, usability and accuracy of the equipment used, as well as to test our resolution routine in combination with the chosen pruning heuristics and their results.

4.1 Test environment

We conducted outdoor experiments on a dry, clear day in the garden. The terrain was flat with some minor surface bumps. We decided to test LIPS system in a topology referenced in Fig. 4.1. Six anchors were evenly spread around the center, forming six radial lines set at an angle of 60 degrees. The radius of the circle was 8 m. Anchors were mounted on a 2 m wooden rod and placed perpendicular to the ground (Fig. 4.2). The actual height of the anchors was determined using a laser distance measurer from a reference point reaching 1 m above the ground. Next, relative coordinates for each anchor (Code 2) were submitted to a target node (Fig. 4.3). Two blind nodes were attached to a lawn mower at different heights. One was at 0.45 m and the other at 0.9 m above the ground. In the experiment we moved the

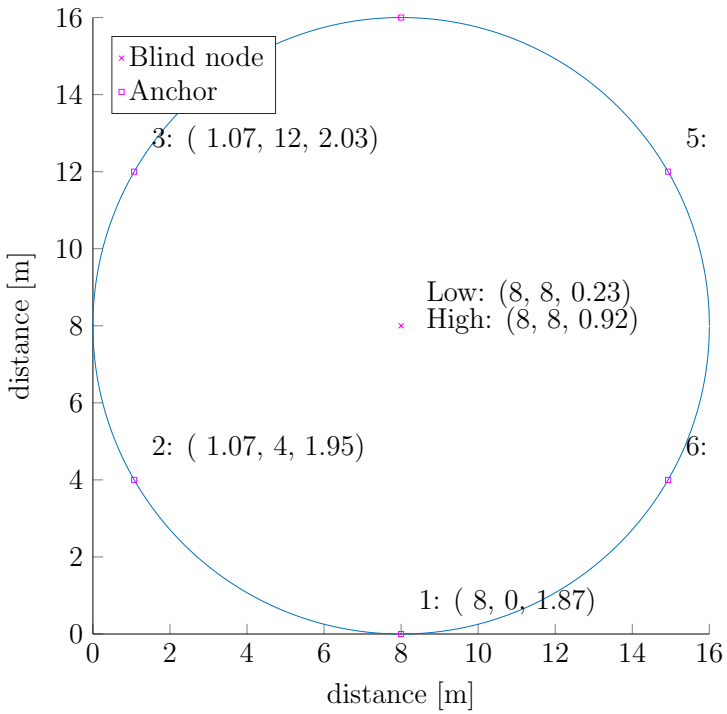

Figure 4.1: A graphical representation of the outdoor topology (floor plan).

lawn mower from the vicinity of a chosen anchor to its direct opposite counter part. A single experiment comprised of one trajectory with 10 s stops at both ends. The lawn mower was moving at a constant speed. Experiments were done in slow and fast pace variation.

4.2 Data analysis

In this section we discuss the unprocessed data collected from the first experiment conducted outdoors. The main goal was to test LIPS equipment and to collect sample data. The graphs show various representations of selected variables.

In Fig. 4.5 the distance to each anchor does not change for the first 11 s because the blind node was not moving. This will be referred as a stationary start. From 11 s to 47 s the node was moved from anchor #4 to anchor #3 in

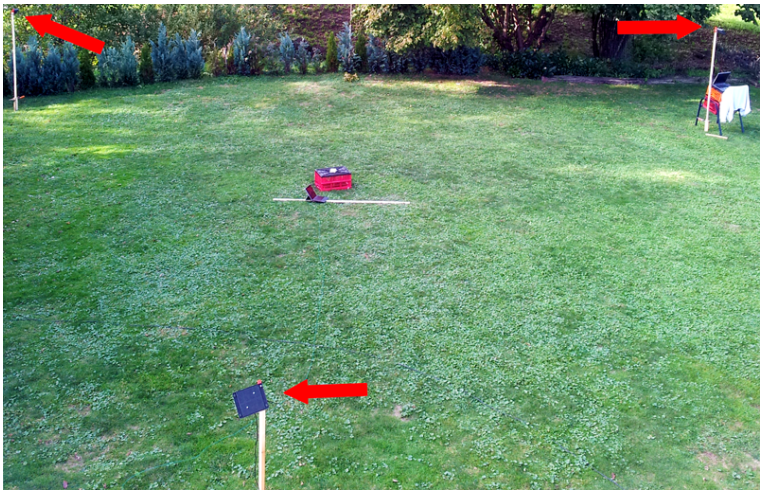

Figure 4.2: The outdoor experiment. Red arrows point to anchor nodes.

Code 2 An example of the configuration procedure for a target node — setting anchor locations.

```
AT+OPMO=1
% Enter configuration mode

AT+AMAP=01,14.93,12,2.1
AT+AMAP=02,8,16,2.1
AT+AMAP=03,1.07,12,2.2
AT+AMAP=04,14.93,4,1.9
AT+AMAP=05,1.07,4,1.9
AT+AMAP=06,8,0,2.1
% [x, y, z] coordinates for each anchor.

AT+STOR=1
% Store the information into persistent storage.

AT+OPMO=0
% Return to normal operation mode.
```

Figure 4.3: Configuring a blind node; the node is connected to a processing unit.

```
+RANG:1246070,6,001,0015.29,0f,002,0000.00,00,003,0001.77,0f,
004,0009.14,0f,005,0011.47,0f,006,0000.00,00
+RANG:1246210,6,001,0015.40,0f,002,0000.00,00,003,0002.03,0f,
004,0009.55,0f,005,-001.00,4b,006,0012.21,0f
```

Figure 4.4: An example of two lines of data received from a blind node.

a straight line at a constant speed. We will refer to this as a moving segment of the experiment. Between 47 s and 53 s there was another stationary period at the end, similar to the stationary start. That concluded our data capture for this experiment.

Due to errors and various interferences during data capture, the data stream was not continuous. This is why there appear to be gaps that break the constant plot flow, which can be seen in Figure 4.5. The bold dots represent GT data. This data is computed on the basis that the starting and end position are known and that, with a constant speed at any point in time, the position of the moving node on the linear trajectory is known. Smaller dots represent the reported distance between the blind node and an anchor.

Figure 4.6 shows the median value marked with an `x` on a vertical line representing the spread between the 10th and 90th percentile. The median and the percentile values are the results of the differences between GT data and the measurements passed through a CDF. The y-axis is intentionally elongated for an easier comparison with the indoor Figure 5.7 discussed in the next chapter.

Due to low errors, the data displayed on the heatmap (Fig. 4.7) visually resembles the path/trajectory between the start and the end point. Each dot represents one line of raw captured data (Fig 4.4) processed by the resolution routine (Eq. (2.1)).

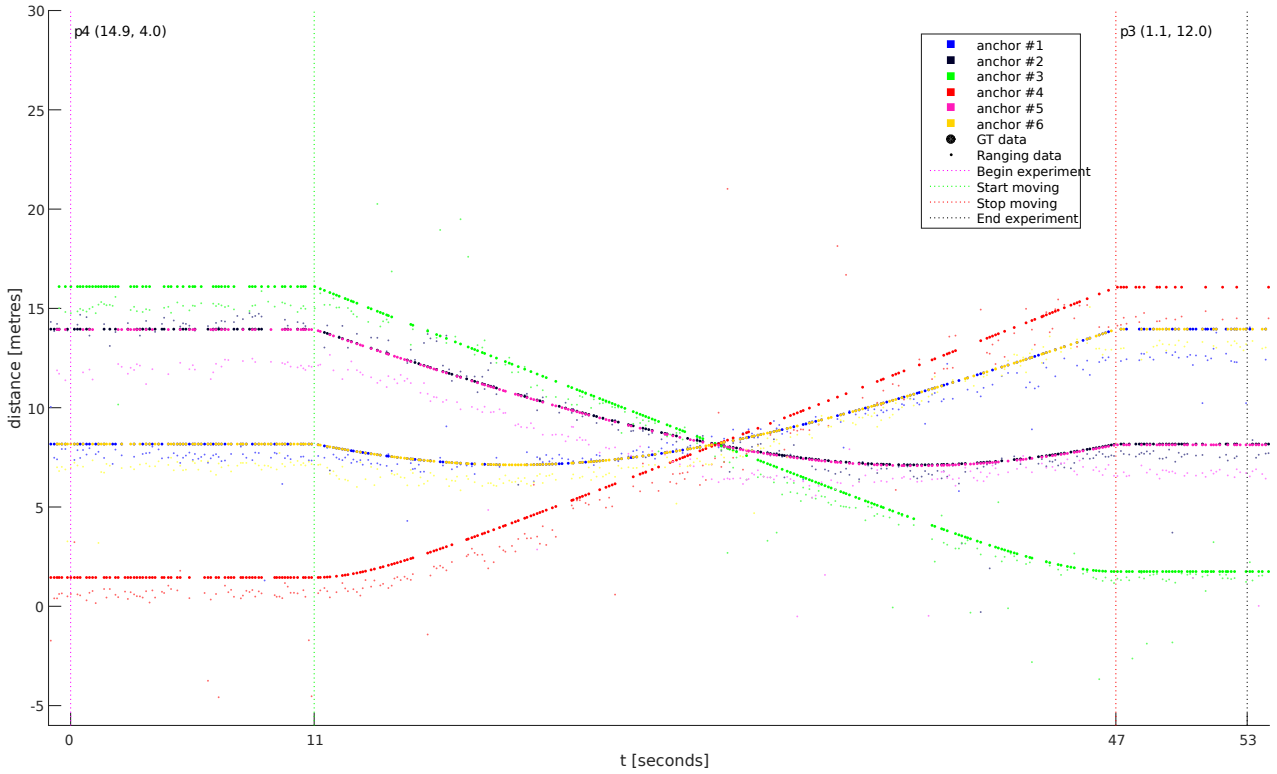

Figure 4.5: The actual (GT) distance between a blind node and an anchor vs. reported ranging data. The L node (height: 0.45 m) — experiment 1 (slow pace). The node is moving from p_4 (anchor #4) to p_3 (anchor #3).

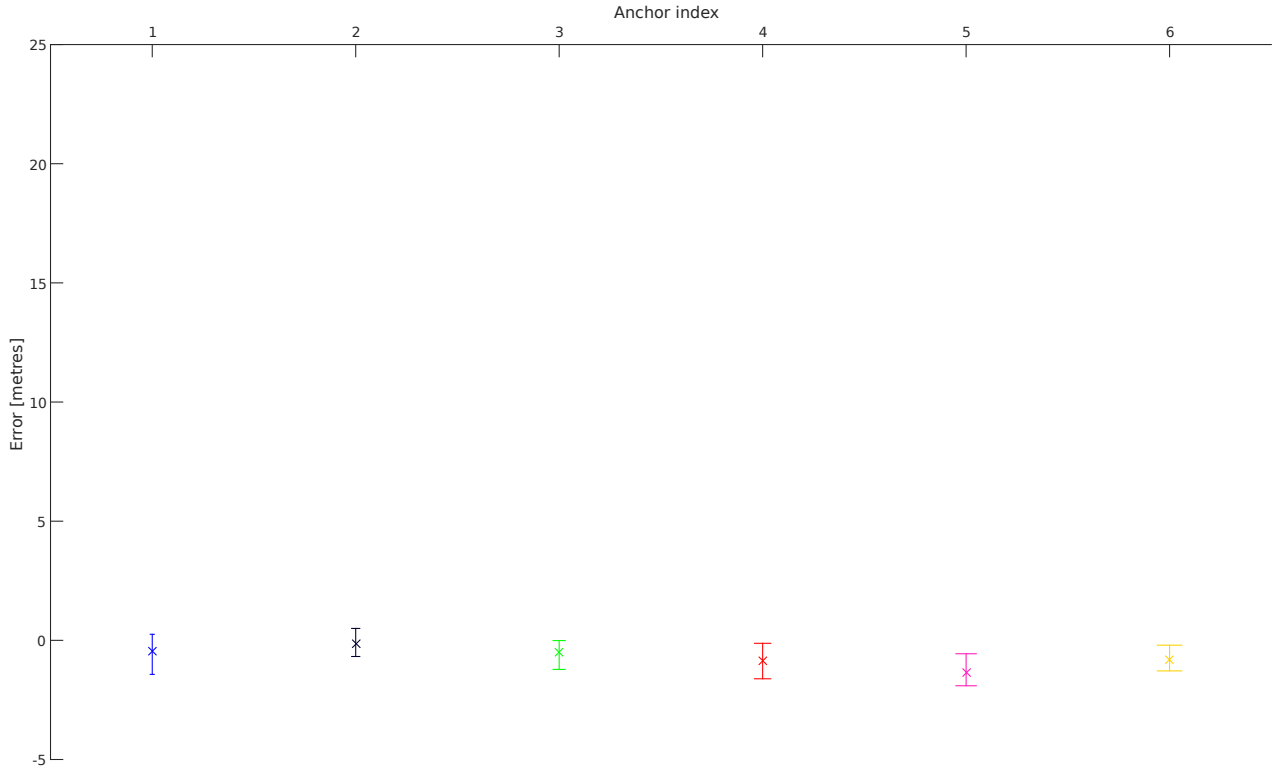

Figure 4.6: Errorbar representation of the distance error between a blind node and an anchor vs. reported ranging data. The L node (height: 0.45 m) — Experiment 1 (slow pace).

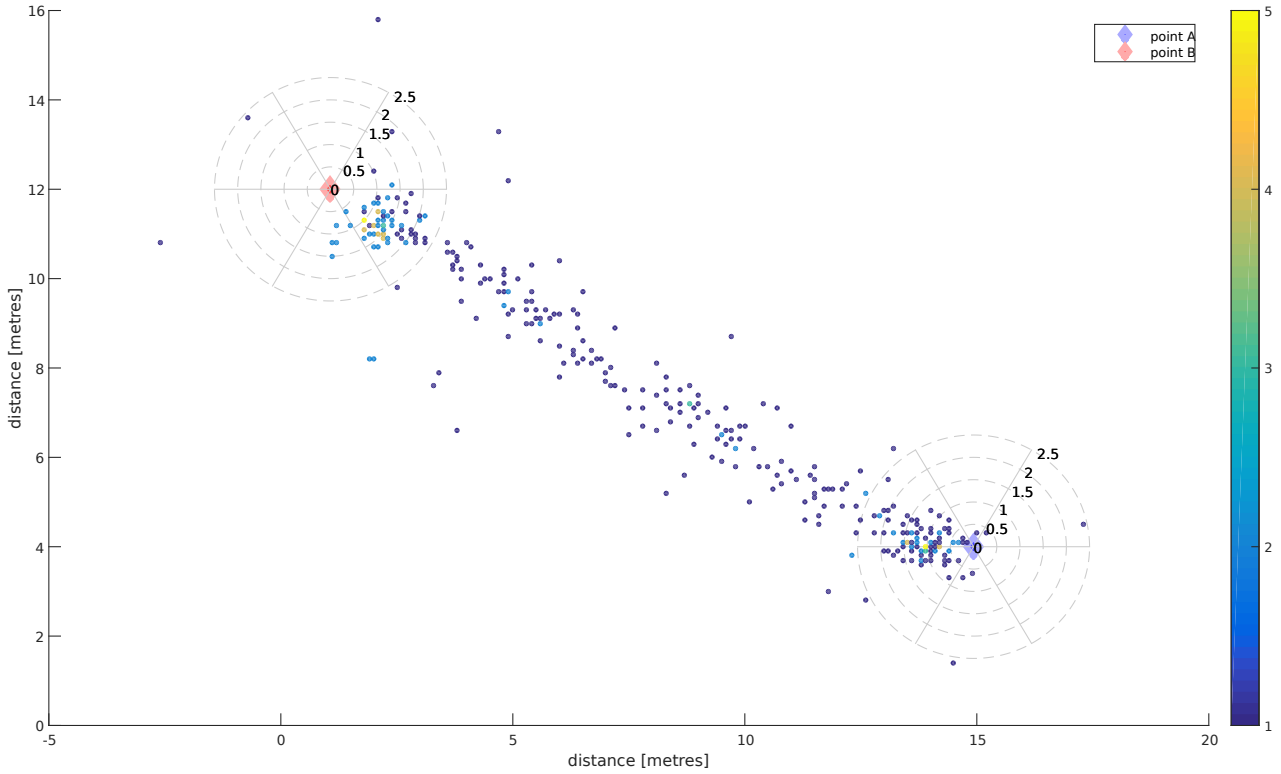

Figure 4.7: A heatmap of point based localization for Experiment 1. The target is moving from point A towards point B at a constant speed. Experiment duration: 53 s.

4.3 Results

This section analyses data obtained from the outdoor experiment which serves as a simplified version of the indoor experiment due to more manageable environment with easier trajectories. The data was processed with various methods and represented graphically. Data for the first experiment is shown in this section, while the rest is presented in the Appendix B because all experiments exhibit a similar pattern.

Figure 4.8 shows the estimated localization from the data collected during the two stationary periods signifying the beginning (in blue) and the end (in red) of the experiment, lasting 11 s and 6 s respectively. Three different statistical pruning methods were used to determine the positions of the blind node. The methods are described in Chapter 2 in sections 2.5.1, 2.5.2, 2.5.3. Statistically, the most prominent pruning heuristic for stationary points turned out to be the robust mean heuristic (Table 4.1). We attribute this to the level of the quality of the measured distances from the majority of the anchors. Distance measurements from almost all the anchors closely resembled the actual (GT) distances (Fig. 4.5). The least accurate position estimates came from the 5th percentile heuristic.

For the moving segment of the experiment (36 s) the resolution routine (Eq. (2.1)) was used to obtain the initial position and the velocity of the blind node as shown in Figure 4.9. To show the trajectory, velocity and duration of the moving segment were multiplied and the results were added to the initial position. To compute the red trajectory, the residual pruning heuristic (Section 2.5.3) was used with a 90 % retention rate to possibly obtain a better fit as opposed to unfiltered data producing the trajectory shown in blue. A mid point was added to the figure (marked by 'x') to mirror the experiment pattern from the computer simulation described in Chapter 3. Surprisingly the most accurate velocity modulus was obtained from raw data without using any pruning heuristic (Table 4.2). We conclude that this is due to the quality of the raw data. However, the closest estimated mid and final point with regard to the GT was obtained using the residual

Table 4.1: Distance errors from the GT position in two stationary points for each heuristic.

Stat. point	*RP*	5th percentile	robust mean
Experiment 1			
p_4	1.23	1.39	0.91
p_3	1.42	2.22	1.24
Experiment 2			
p_3	1.82	3.18	2.04
p_4	0.86	2.30	0.53
Experiment 3			
p_1	1.47	2.70	1.35
p_5	0.61	2.18	0.67
Experiment 4			
p_5	2.09	2.07	1.61
p_1	0.83	2.02	0.61
Averages			
	1.29	2.26	1.12

pruning heuristic with the retention of 90 %.

Table 4.2: Tabular representation of the results for the moving segments. The table shows GT velocity and three computed velocities. The average velocities are obtained by averaging the absolute error between GT velocity and the computed ones. The mid and final point columns show distance errors from the GT position, respectively.

Traj. index	velocity				mid point			final point		
	GT	FT	RP_{80}	RP_{90}	FT	RP_{80}	RP_{90}	FT	RP_{80}	RP_{90}
Experiment 1 (slow)										
1	0.44	0.42	0.40	0.40	0.34	0.43	0.39	0.42	0.58	0.63
Experiment 2 (fast)										
1	0.99	1.04	0.92	0.94	1.25	0.46	0.70	1.68	0.44	0.27
Experiment 3 (slow)										
1	0.48	0.46	0.44	0.45	0.47	0.66	0.47	0.42	1.23	0.60
Experiment 4 (fast)										
1	1.00	0.98	0.86	0.90	1.23	0.83	0.69	1.12	0.45	0.31
Averages										
		0.03	0.07	0.05	0.82	0.60	0.56	0.91	0.67	0.46

The estimated trajectory lines exhibit a noticeable departure from the ground truth (in grey). The disparity values in mid points for all four experiments were used as an error metric for the CDF in Figure 4.10, while in Figure 4.11 the stationary points were also included in the plot.

Figures 4.12 and 4.13 show RMS error in relation to the velocity modulus. In the simulation results (Fig. 3.4, 3.5) the relation between the velocity modulus and the position error was observed; however, in the applied experiments the number of trials was too low to establish a statistical correlation.

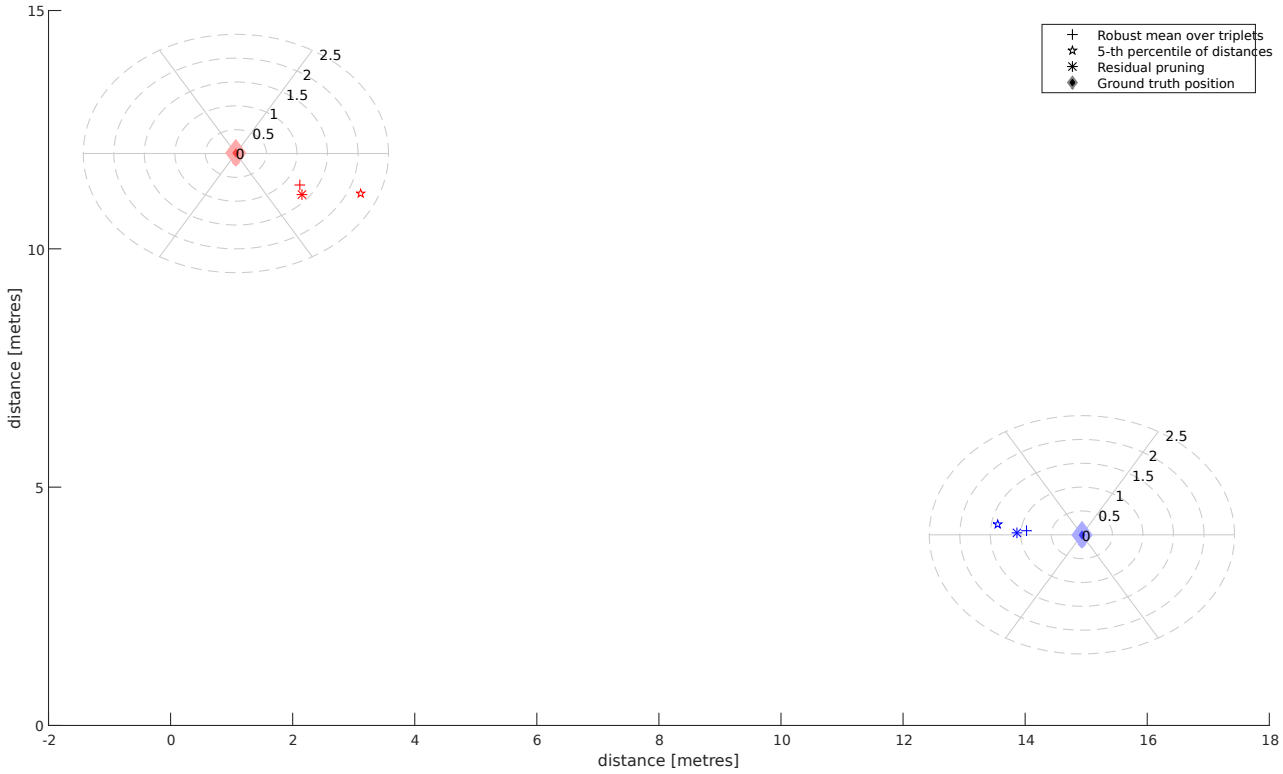

Figure 4.8: Static position estimation for the L node (height: 0.45 m) — Experiment 1 (slow pace). Residual pruning retention rate: 90 %, robust mean with a 50 % retention rate.

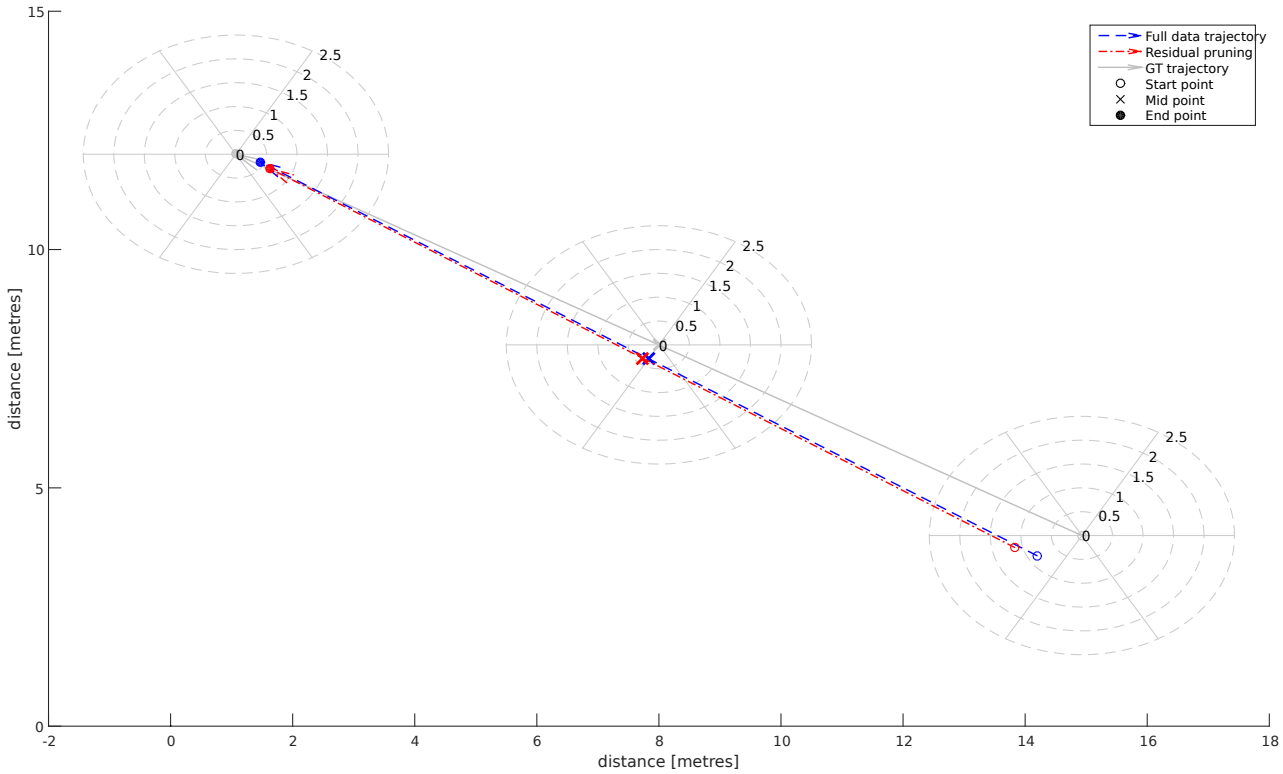

Figure 4.9: Trajectory estimation for the L node (height: 0.45 m) — Experiment 1 (slow pace). Residual pruning retention rate: 90 %.

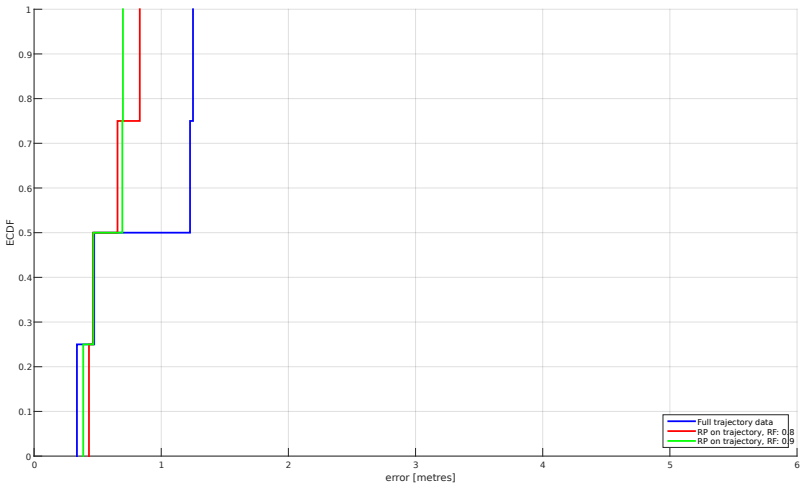

Figure 4.10: CDF on mid points.

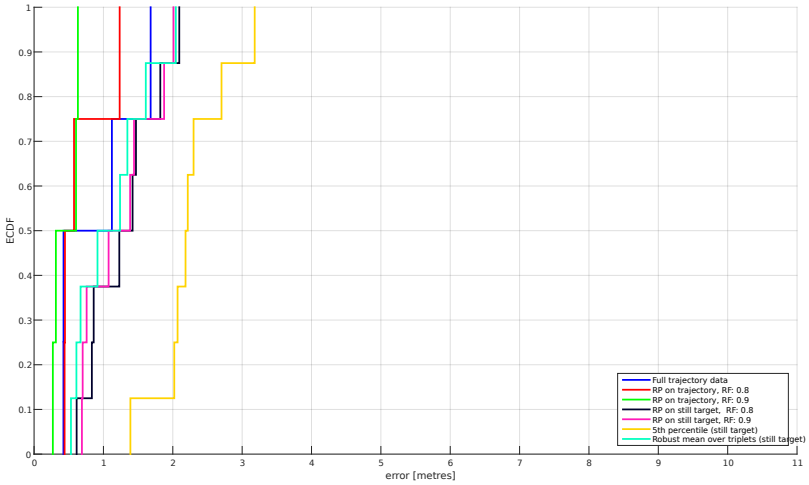

Figure 4.11: CDF on initial and final points.

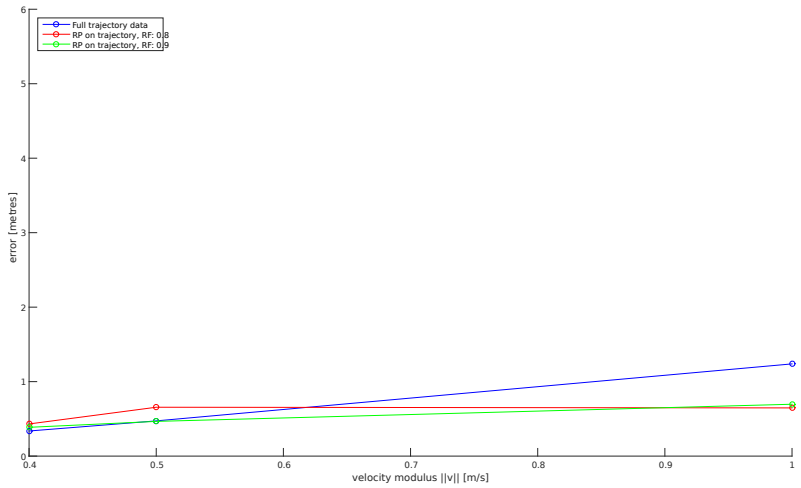

Figure 4.12: Velocity modulus vs. RMS error on mid points.

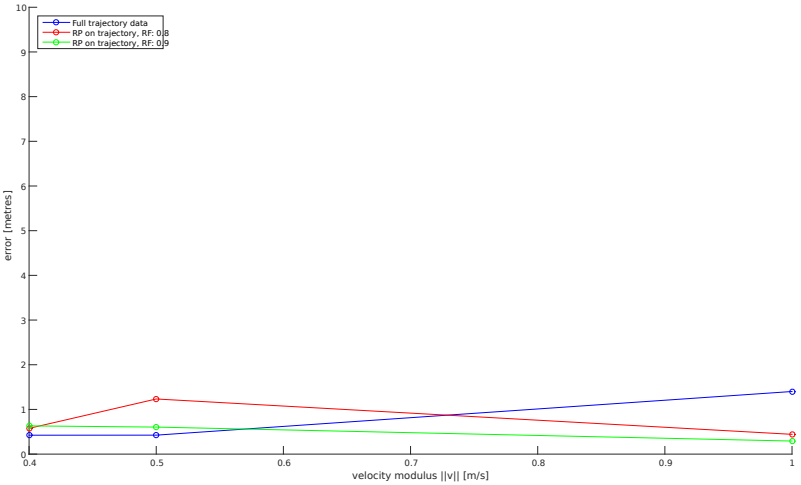

Figure 4.13: Velocity modulus vs. RMS error on final points.

Chapter 5

Indoor experiments

The indoor experiments that were conducted are meant to reflect a real life situation where a system like this might be used. This chapter deals with data captured from a selected indoor experiment, its analysis and discusses the outcomes of resolution methods described in the Problem formulation (Chapter 2).

5.1 Test environment

Indoor experiments were conducted in the empty faculty cafeteria. This location was chosen because it is spacious and has a high ceiling. Six anchors were placed on the ceiling with antenna facing downwards. Anchors were at different heights (3.9 m - 4.5 m) because the roof is inclined towards one end. Coverage area of an anchor can be calculated as following: $R = H \tan(60°)$, where R is the radius of area covered on the ground and H is the anchor height. All anchors' position were projected on the floor using a laser measurer and marked with an 'X' (Figs. 5.1 and 5.3) in order to get the anchors' exact heights. The distance between anchor A_5 and anchor A_6 served as a referential segment. Other anchors' coordinates were obtained by measuring their perpendicular distance onto our referential segment as shown in Figure 5.4. Coordinates were, as before, submitted to the blind nodes. An

Figure 5.1: The indoor experiment. Red arrows point to the anchor nodes.

Intravenous (IV) pole (Fig. 5.2) served as an improvised moving object with two blind nodes attached at the height of 1.3 m (the L node) and 2 m (the H node), respectively. The lower blind node was mounted with its antenna facing perpendicular to the ground, while the upper node antenna faced upwards.

A tour is a sequence of segments. Three different tours were designed (Fig. 5.5) and conducted at two different paces, resulting in six independent experiments. The idea was to test areas covered with many anchors as well as areas with obstructions, corners and similar which is reflected in the tour patterns. Keypoints of the tours were labeled with markers on the ground (Fig. 5.3). The coordinates of these keypoints were assigned with the aid of the aforementioned referential segment. The IV pole was moved along these segments with a constant speed at a slow and a faster pace. Ten second stops were made at each keypoint. Simultaneously, ranging information was captured from the blind nodes.

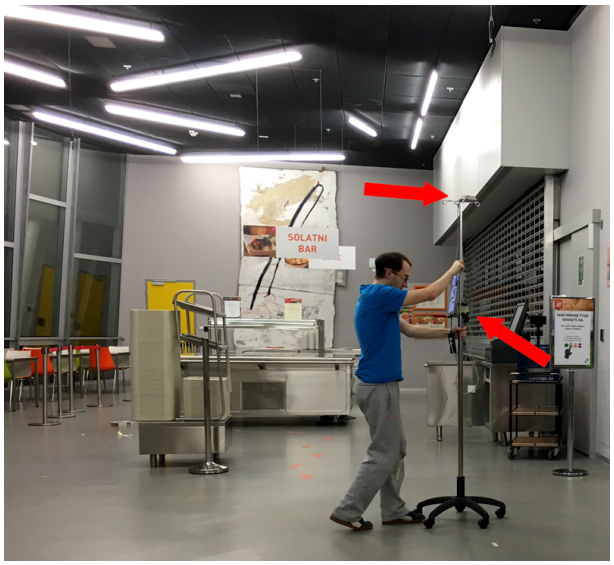

Figure 5.2: Position of the nodes on the IV pole.

Figure 5.3: Markers.

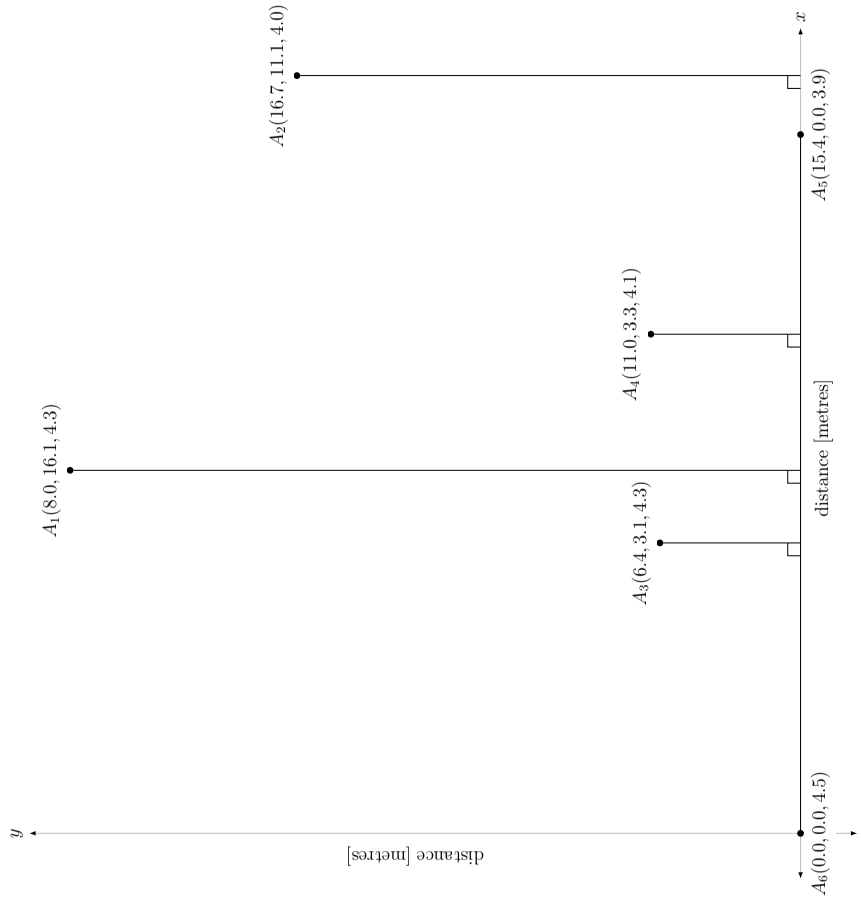

Figure 5.4: The indoor anchor layout (represented with the coordinates [x, y, z]). The reference segment is defined by the anchors A_5 and A_6.

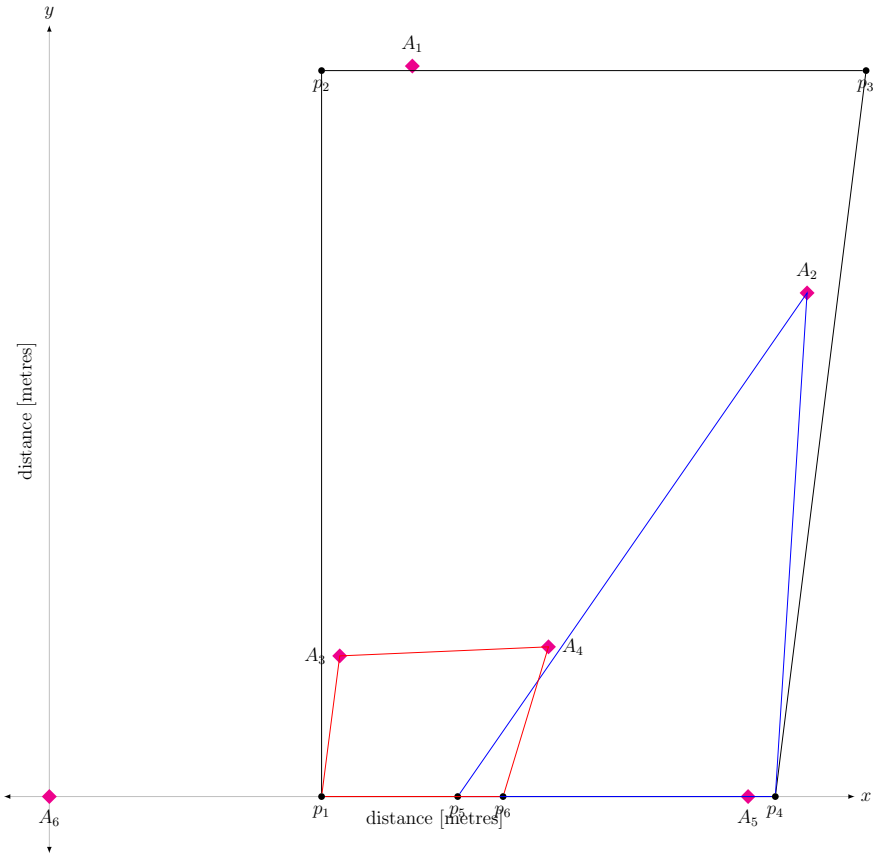

Figure 5.5: Three tours. $T_1 = \{p_1, p_2, p_3, p_4, p_1\}$, $T_2 = \{p_5, A_2, p_4, p_5\}$ and $T_3 = \{p_1, A_3, A_4, p_6, p_1\}$. The anchor nodes are depicted in magenta diamonds, some of which some served as keypoints. Other keypoints are labelled p_1 to p_6.

5.2 Data analysis

Figure 5.6 shows the data collected from Tour 1 at a faster pace. As with the outdoor experiment, the movement is divided into moving and stationary segments of various duration. A stationary segment starts with a red vertical separator and ends with a green vertical separator. The opposite is true for the moving segments. During the stationary periods the distance stays roughly the same, which can be concluded from the plot.

The first 69 s of the experiment are represented in Fig 5.7, only this time the distance error between the blind node and the anchors is shown using the same procedure applied to the outdoor experiment (Fig. 4.6). The same temporal segment was analyzed using point based localization as well to yield a heatmap (Fig. 5.8).

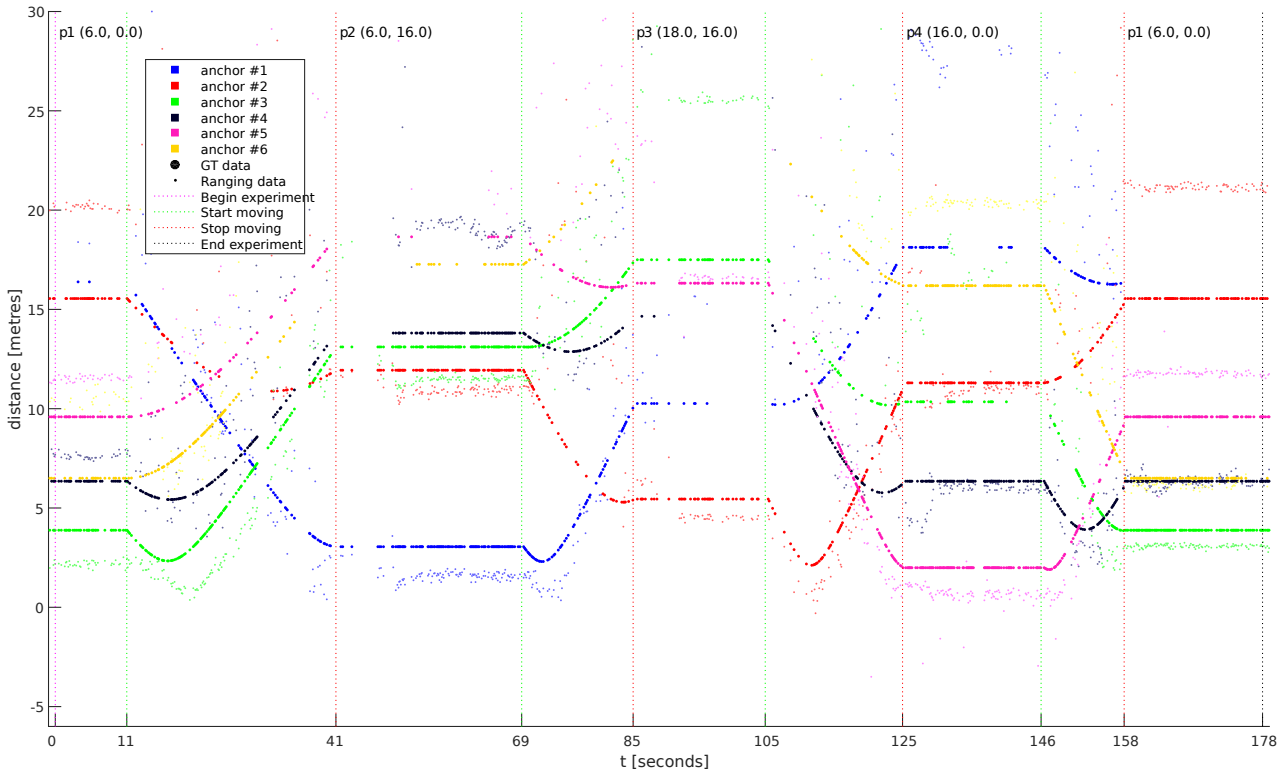

Figure 5.6: The GT distance between a blind node and an anchor vs. reported ranging data. The H node (height: 2 m) — Experiment 2 (fast pace).

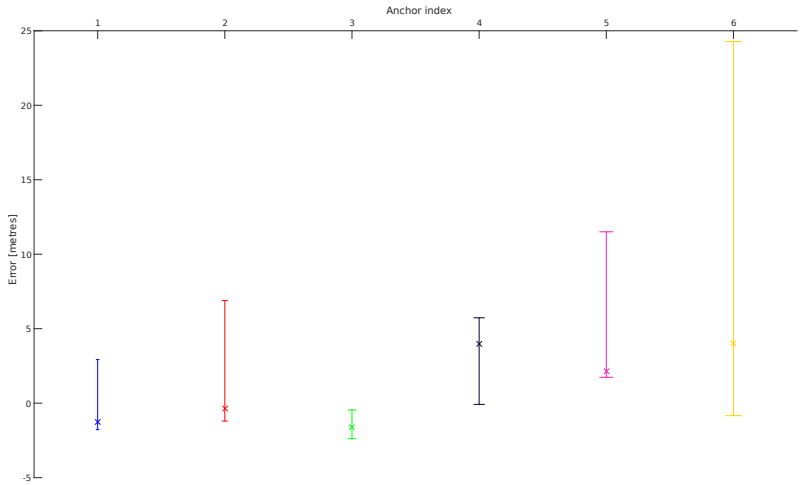

Figure 5.7: Errobar representation of the distance error between a blind node and an anchor vs. reported ranging data. The H node (height: 2 m) — Experiment 2 (fast pace), the first trajectory.

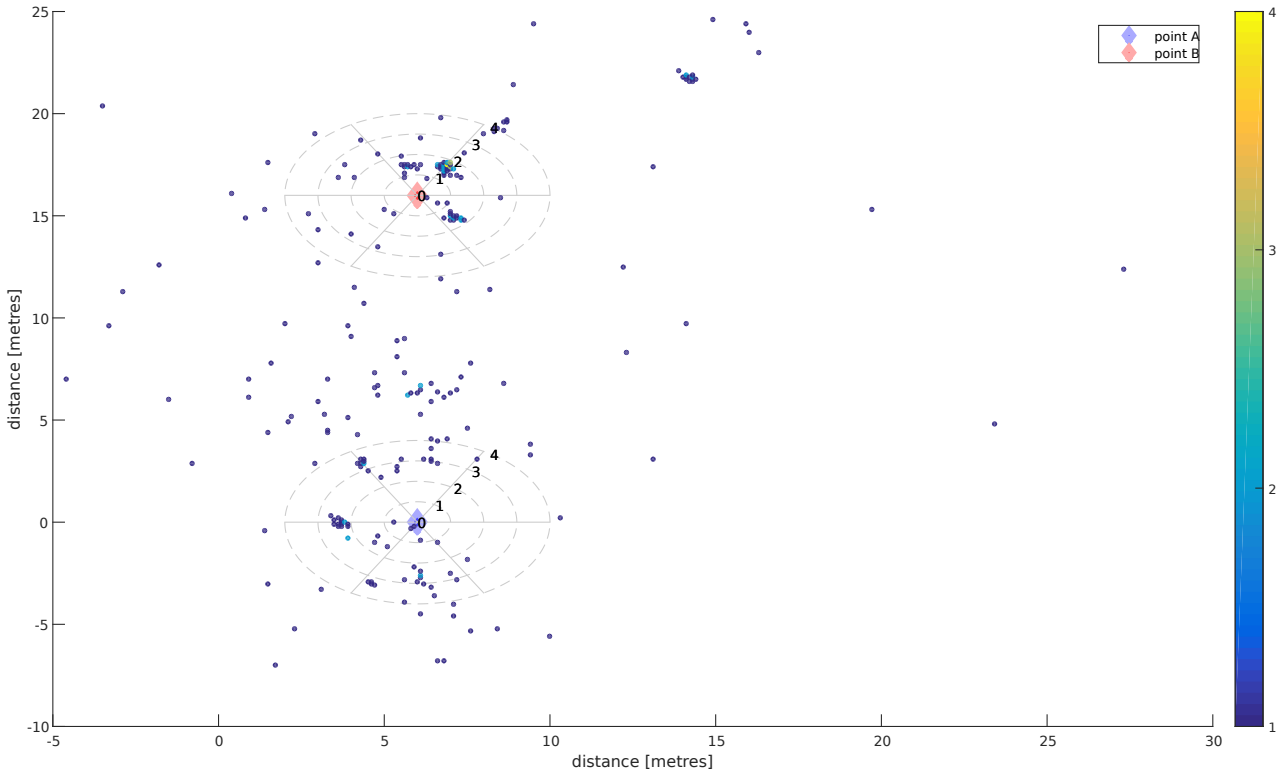

Figure 5.8: A heatmap of point based localization for the first trajectory of Experiment 2. The target node is moving from point A towards point B at a constant speed. Segment duration: 69 s (including both stops).

5.3 Results and discussion

The indoor experiments were more complex compared to the introductory one discussed in Chapter 4, where we did not deal with multiple trajectories in a single experiment. The data collected during the experiments was greatly influenced by the coverage interference caused by the nearby walls and anchor blind spots. As in the previous chapter, the same heuristic pruning methods were used.

At the stationary periods the collected data was analyzed using three pruning heuristics as in the previous chapter. Figure 5.9 is the graphical representation of the results. Polar charts map the distance error from the GT location at each stationary point. Each symbol represents a different statistical pruning heuristic. The greatest deviations from the GT were found in red and green stationary periods. This was attributed to low anchor coverage. Overall, the best results were obtained by the residual pruning heuristic, represented with an asterisk. While the other two heuristics were inferior to the residual pruning heuristic they both yielded comparable results. A more detailed representation is shown in Table 5.1.

Moving periods for Experiment 2 are represented in Figure 5.10. For all other experiments, the analysis of the stationary as well as moving segments is presented in the Appendix C. When moving towards keypoints with poor anchor coverage, trajectory errors increase. In general, the direction of the trajectories reflected the GT, whereas trajectory scalar values were overestimated. The best optimization of the full data trajectories was achieved using the residual pruning heuristic with the retention rate of 80 % (Table 5.2). The mid points for all experiments were used to generate CDF in Figure 5.11. Figure 5.12 combines localization of the stationary segments and trajectories' final point estimates. RMS errors were also computed; however, due to a low number of trials, the results are inconclusive (Figs. 5.13, 5.14).

Table 5.1: Distance errors from the GT position in all stationary points for each heuristic.

Stat. point	RP	5th percentile	robust mean
Experiment 1			
p_1	2.39	3.34	2.29
p_2	0.87	1.81	0.82
p_3	7.75	5.26	7.21
p_4	1.15	2.65	1.56
p_1	3.65	6.45	6.67
Experiment 2			
p_1	2.14	1.90	2.14
p_2	1.17	9.02	0.66
p_3	3.51	5.79	5.80
p_4	0.73	2.41	1.31
p_1	3.82	1.73	2.61
Experiment 3			
p_5	2.79	0.22	1.38
A_2	2.89	5.07	7.04
p_4	0.43	2.45	0.67
p_5	1.12	1.00	1.66
Experiment 4			
p_5	4.26	5.09	4.86
A_2	1.11	3.08	2.42
p_4	3.48	3.54	3.66
p_5	2.21	3.04	2.49
Experiment 5			
p_1	5.61	1.19	6.68
A_3	0.61	1.94	0.60
A_4	0.79	0.94	1.18
p_6	5.01	0.85	3.55
p_1	5.56	5.42	5.91
Experiment 6			
p_1	2.17	5.69	3.14
A_3	1.33	1.30	1.04
A_4	0.68	0.43	0.54
p_6	2.11	0.67	2.21
p_1	2.55	7.24	9.69
Averages			
	2.57	3.20	3.21

Table 5.2: Tabular representation of the results for the moving segments. The table shows GT velocity and three computed velocities. The average velocities are obtained by averaging the absolute error between GT velocity and the computed ones. The mid and final point columns show distance errors from the GT position, respectively.

Traj. index	velocity				mid point			final point		
	GT	FT	RP_{80}	RP_{90}	FT	RP_{80}	RP_{90}	FT	RP_{80}	RP_{90}
Experiment 1 (slow)										
1	0.30	0.39	0.31	0.34	2.35	0.26	1.10	4.60	0.21	2.06
2	0.26	0.29	0.31	0.31	5.67	3.25	3.95	10.42	8.71	8.28
3	0.25	0.33	0.29	0.31	3.22	0.83	1.60	3.42	1.52	2.55
4	0.27	0.35	0.34	0.34	1.94	0.69	0.94	0.84	1.52	0.40
Experiment 2 (fast)										
1	0.52	0.75	0.59	0.63	1.49	0.69	1.12	4.10	0.51	1.57
2	0.73	0.69	0.82	0.79	5.82	3.09	4.79	9.85	6.91	9.49
3	0.80	0.96	0.84	0.90	3.40	0.94	1.90	3.25	1.15	1.36
4	0.83	1.14	1.06	1.14	1.97	0.75	1.01	1.00	1.49	0.88
Experiment 3 (slow)										
1	0.26	0.31	0.24	0.26	0.77	0.27	0.24	2.01	0.32	0.37
2	0.24	0.33	0.30	0.33	3.42	1.17	1.83	2.92	1.06	2.04
3	0.23	0.30	0.31	0.30	2.47	0.79	1.31	1.26	0.81	0.79
Experiment 4 (fast)										
1	0.64	0.80	0.63	0.70	1.22	0.32	0.48	3.01	0.33	1.24
2	0.56	0.89	0.70	0.82	3.02	1.05	1.73	3.33	1.27	2.10
3	0.76	1.25	0.97	1.01	2.40	1.09	1.17	0.71	1.00	0.47
Experiment 5 (slow)										
1	0.23	0.41	0.13	0.10	0.63	1.09	1.60	0.95	0.41	0.69
2	0.34	0.29	0.31	0.34	0.09	0.16	0.37	0.41	0.15	0.31
3	0.32	0.31	0.14	0.23	1.02	1.26	0.74	1.25	2.30	1.20
4	0.30	0.27	0.47	0.47	0.82	1.49	0.38	0.98	2.35	1.60
Experiment 6 (fast)										
1	0.76	0.96	0.51	0.53	1.83	2.07	2.26	2.05	1.06	1.29
2	0.95	1.02	1.04	1.25	0.55	0.09	0.38	0.71	0.34	0.50
3	0.93	1.28	0.51	1.16	1.54	0.95	0.68	2.35	1.70	0.86
4	0.94	0.81	1.42	1.88	0.67	2.36	2.05	0.62	3.78	5.28
Averages										
		0.15	0.12	0.16	2.11	1.12	1.44	2.73	1.77	2.06

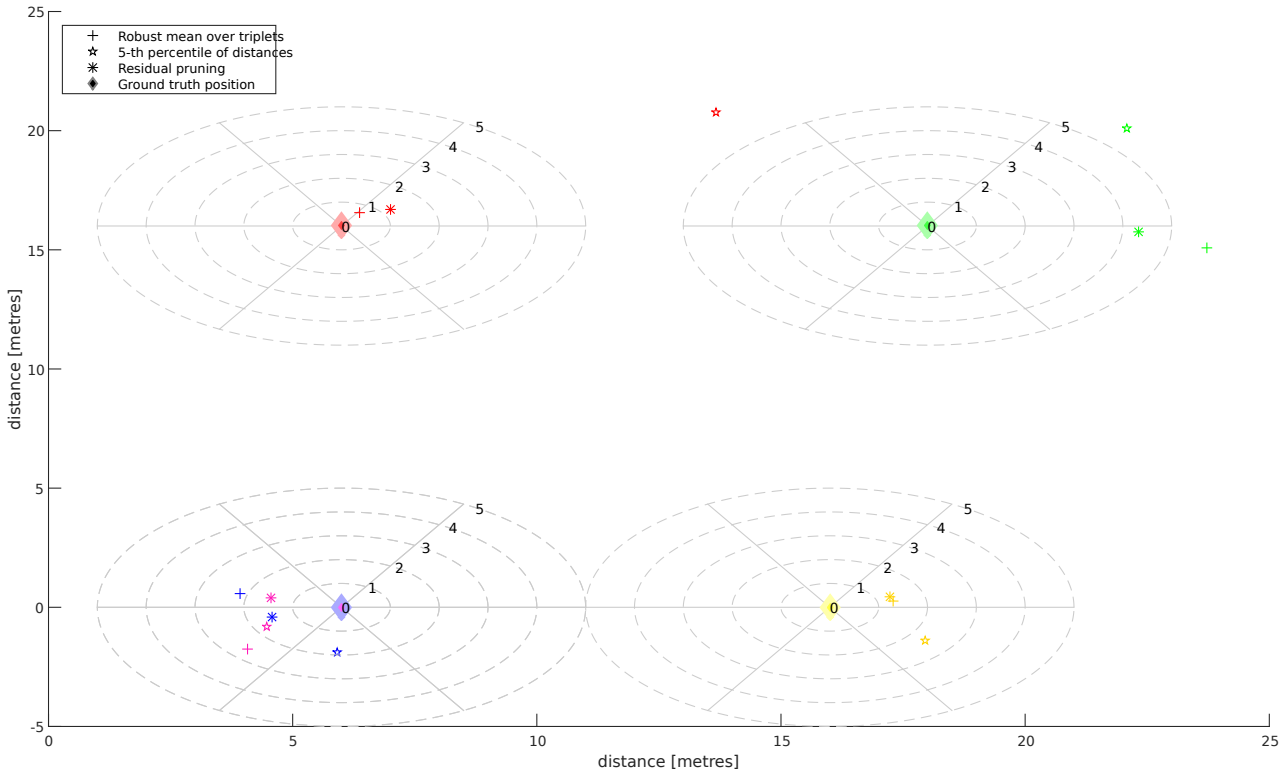

Figure 5.9: Static position estimation for the H node at the height of 2 m — Experiment 2 (fast pace). Residual pruning retention rate: 90 %, robust mean with a 50 % retention rate.

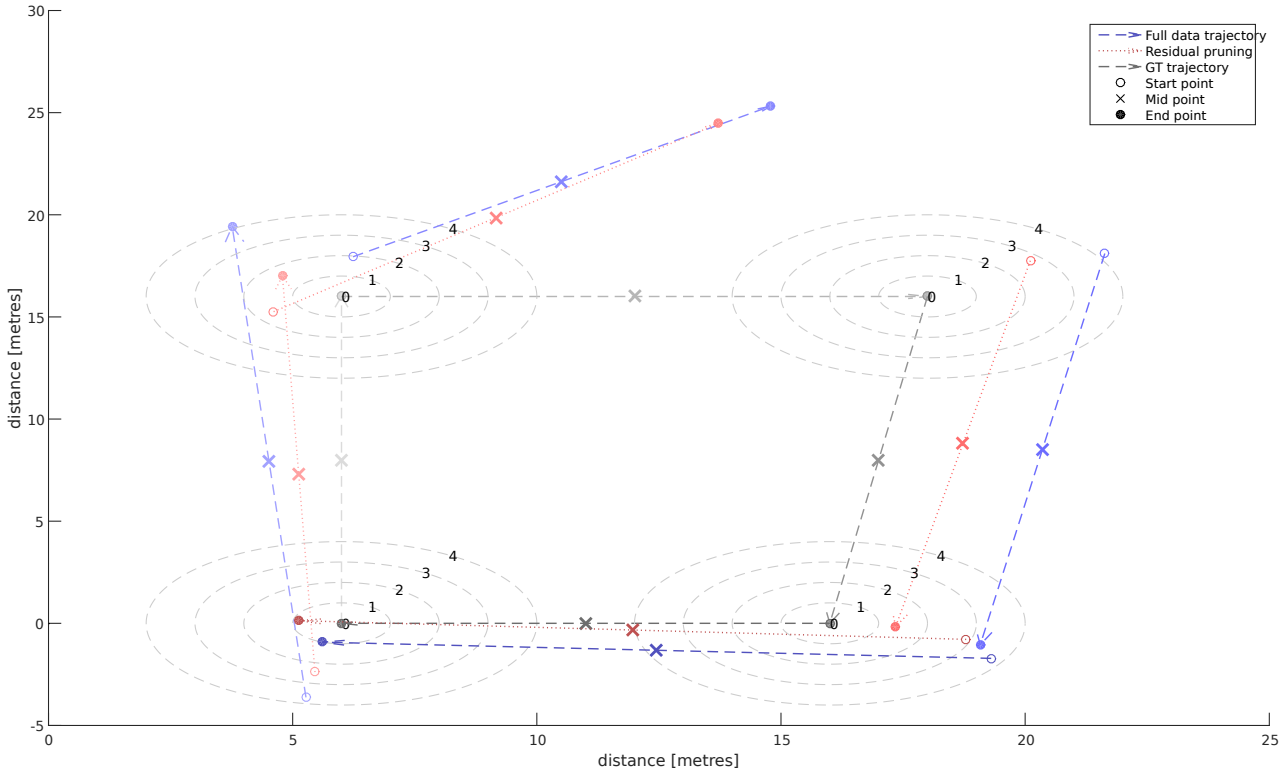

Figure 5.10: Experiment 2 (fast pace) trajectories with the H node (height: 2 m). Residual pruning retention rate: 90 %. Opacity indicates the course of the experiment, trajectories fade with time.

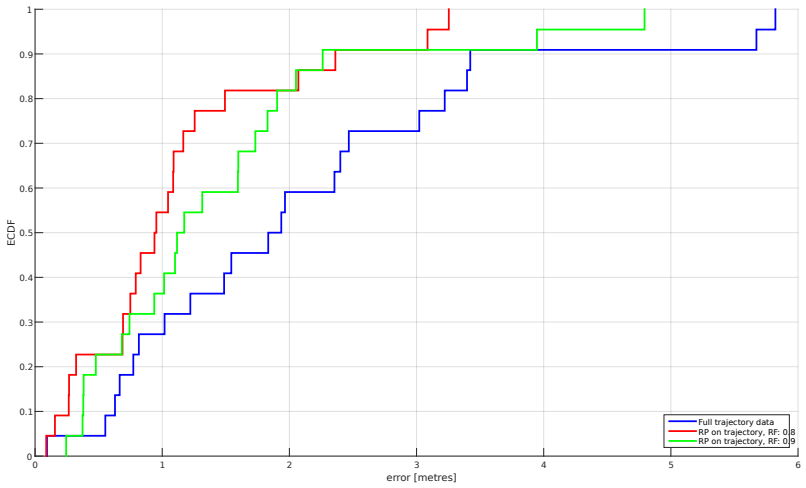

Figure 5.11: CDF on mid points.

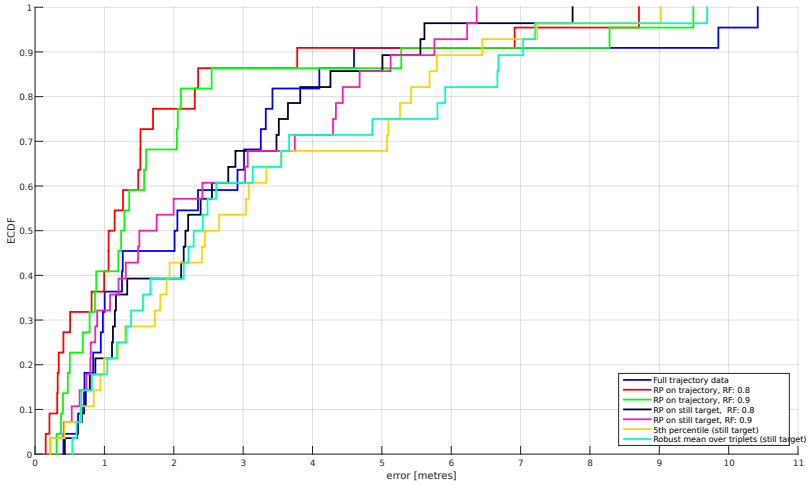

Figure 5.12: CDF on final points.

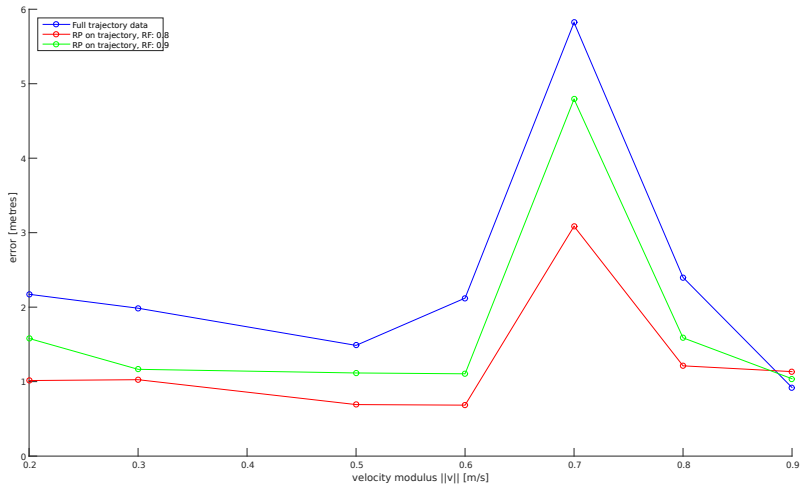

Figure 5.13: Velocity modulus vs. RMS error on mid points.

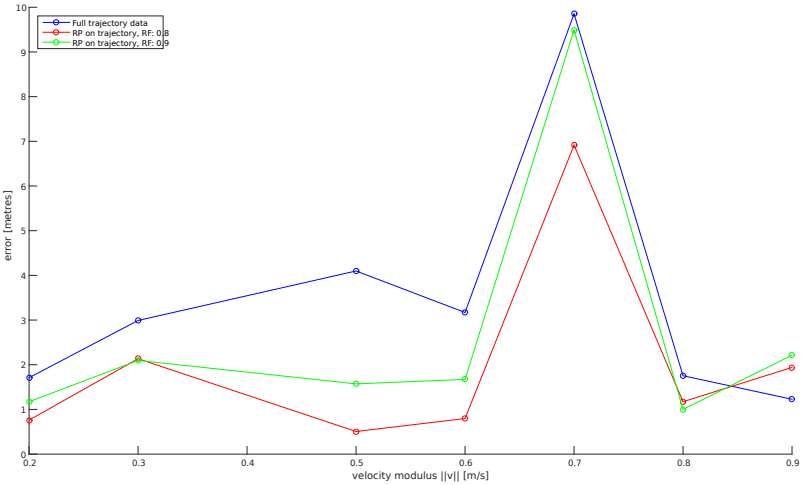

Figure 5.14: Velocity modulus vs. RMS error on final points.

Chapter 6

Conclusions

This work elaborates trajectory based localization. The goal of the thesis was to determine a blind node's trajectory, defined as a function of its initial position and its velocity in a given time frame. The resolution routine, the input of which are the ranging measurements from the industrial, scientific and medical radio band, used to estimate the trajectory parameters is the optimization of the non-linear least squares model. Additional statistical pruning heuristics were combined with our resolution routine to filter the biggest outlying measurements.

Simulation results unexpectedly implied that the distance error linearly increases with the velocity modulus, yet to confirm this claim in a physical environment, further testing is required. Moreover, the simulation indicated that the best results are obtained within the convex polygon formed by the anchors. For the practical part of this thesis a simple outdoor experiment was carried out to test LIPS equipment. The results closely reflected the ground truth.

On the contrary, a more complex indoor experiment showed greater errors compared to the outdoor one. The indoor environment presented a greater set of challenges for the system in determining the location of the blind node. Various elements influenced the accuracy of the data regarding the blind node's position.

Overall, the most resilient heuristic of residual pruning turned out to be the most accurate for stationary as well as moving segments. With this heuristic, 90 % of all distance errors were under 4 m, which is in range with indoor positioning systems that are currently available on the market. The heuristics used during the experiments were able to handle small and symmetric distance error anomalies. Although there was a moderate success with the described pruning heuristics in combating the lack of line of sight in a harsh indoor environment, it is up to the manufacturer to filter out multipath signals as the phenomenon is detected on the physical level.

Regarding our initial prediction that our 5th percentile heuristic would perform better in the indoor environment due to its ability to handle bimodal distribution, we are now able to confirm its designated function. Still, this heuristic was greatly inferior to the residual pruning heuristic.

For further work on this topic we suggest that our localization pipeline be used with other wireless technologies. Since our testing equipment was very expensive and small scale, using more widely implemented technologies, i.e. cellular networks, bluetooth, WLAN, etc., would provide us with a valuable comparison for determining the appropriateness of these low cost solutions as indoor positioning systems.

Bibliography

[1] A. Coluccia, F. Ricciato, On ML estimation for automatic RSS-based indoor localization, in: 2010 5th IEEE International Symposium on Wireless Pervasive Computing (ISWPC), IEEE, 2010, pp. 495–502.

[2] A. Coluccia, F. Ricciato, Maximum likelihood trajectory estimation of a mobile node from RSS measurements, in: 2012 9th Annual Conference on Wireless On-demand Network Systems and Services (WONS), IEEE, 2012, pp. 151–158.

[3] Official U.S. Government information about the Global Positioning System (GPS) and related topics.
URL `http://www.gps.gov`

[4] B. Hofmann-Wellenhof, H. Lichtenegger, J. Collins, Global positioning system: theory and practice, Springer Science & Business Media, 2012, Ch. Overview of GPS, pp. 11–25.

[5] A. Kleusberg, R. B. Langley, The limitations of GPS, *GPS World* **1.2**, 1990.

[6] N. Facchi, F. Gringoli, F. Ricciato, A. Toma, Emitter localisation from reception timestamps in asynchronous networks, *Computer Networks* **88**, Elsevier, 2015, pp. 202–217.

[7] H. Zou, H. Wang, L. Xie, Q.-S. Jia, An RFID indoor positioning system by using weighted path loss and extreme learning machine, in: 2013

IEEE 1st International Conference on Cyber-Physical Systems, Networks, and Applications (CPSNA), IEEE, 2013, pp. 66–71.

[8] B. S. Lakmali, D. Dias, Database correlation for GSM location in outdoor & indoor environments, in: 2008 4th International Conference on Information and Automation for Sustainability, ICIAFS 2008, IEEE, 2008, pp. 42–47.

[9] M. Kuhn, C. Zhang, B. Merkl, D. Yang, Y. Wang, M. Mahfouz, A. Fathy, High accuracy UWB localization in dense indoor environments, in: 2008 IEEE International Conference on Ultra-Wideband, ICUWB 2008, Vol. 2, IEEE, 2008, pp. 129–132.

[10] C. Frost, C. S. Jensen, K. S. Luckow, B. Thomsen, R. Hansen, Bluetooth indoor positioning system using fingerprinting, in: Mobile lightweight wireless systems, Springer, 2011, pp. 136–150.

[11] H. Liu, H. Darabi, P. Banerjee, J. Liu, Survey of wireless indoor positioning techniques and systems, *IEEE Transactions on Systems, Man, and Cybernetics, Part C: Applications and Reviews* **37.6**, IEEE, 2007, pp. 1067–1080.

[12] S. Lanzisera, D. Zats, K. S. Pister, Radio frequency time-of-flight distance measurement for low-cost wireless sensor localization, *IEEE Sensors Journal* **11.3**, IEEE, 2011, pp. 837–845.

[13] M. Ltd., LIPS Local Indoor Positioning System (2015).
URL `https://www.multilux.eu/docs/MRFUM01.pdf`

[14] N. T. GmbH, Real time location systems (rtls), in: A White Paper from Nanotron Technologies GmbH, Nanotron Technologies GmbH, 2007.
URL `http://www.nanotron.com/EN/pdf/WP_RTLS.pdf`

[15] J. Xiong, K. Sundaresan, K. Jamieson, Tonetrack: Leveraging frequency-agile radios for time-based indoor wireless localization, in:

Proceedings of the 21st Annual International Conference on Mobile Computing and Networking, ACM, 2015, pp. 537–549.

[16] S. Marano, W. M. Gifford, H. Wymeersch, M. Z. Win, NLOS identification and mitigation for localization based on UWB experimental data, *IEEE Journal on Selected Areas in Communications* **28.7**, IEEE, 2010, pp. 1026–1035.

[17] Y. Bar-Shalom, X. R. Li, T. Kirubarajan, Estimation with applications to tracking and navigation: theory algorithms and software, John Wiley & Sons, 2004.

Appendix A

Preliminary simulations

A.1 CDF

This section presents figures of cumulative distribution function of distance errors on mid and final point, obtained with our resolution routine using various noise variables during computer simulations. Four area cases are superimposed on each figure.

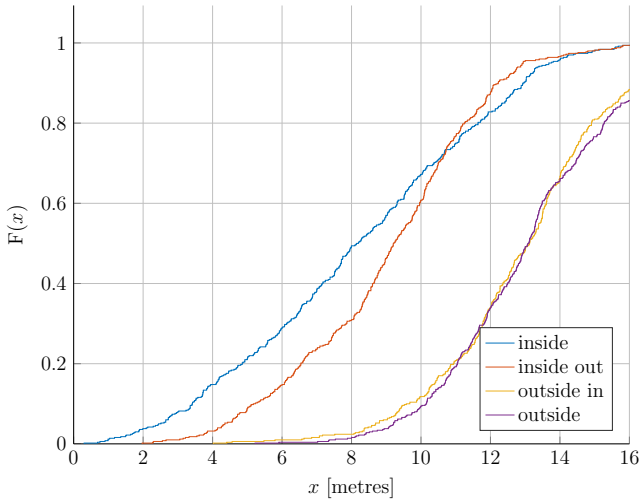

Figure A.1: CDF for FMUg on mid points, $\sigma = 5, \alpha = 0.5, \beta = 0.5$.

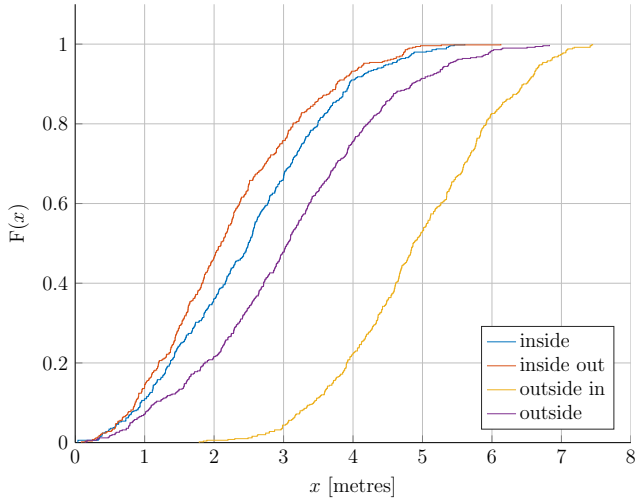

Figure A.2: CDF for FMUg on mid points, $\sigma = 5, F = 10$.

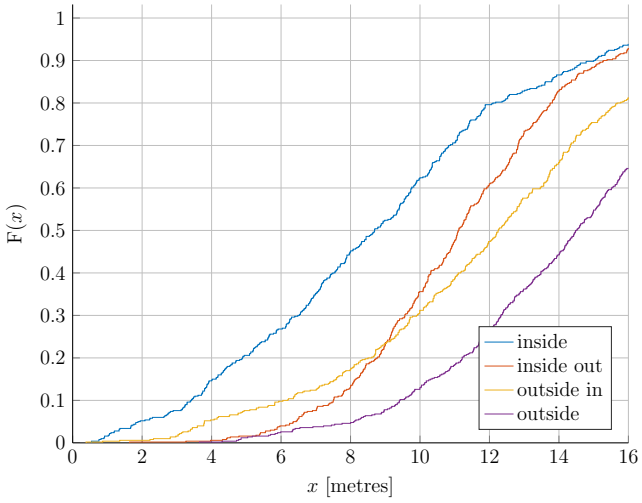

Figure A.3: CDF for FMUg on final points, $\sigma = 5, \alpha = 0.5, \beta = 0.5$.

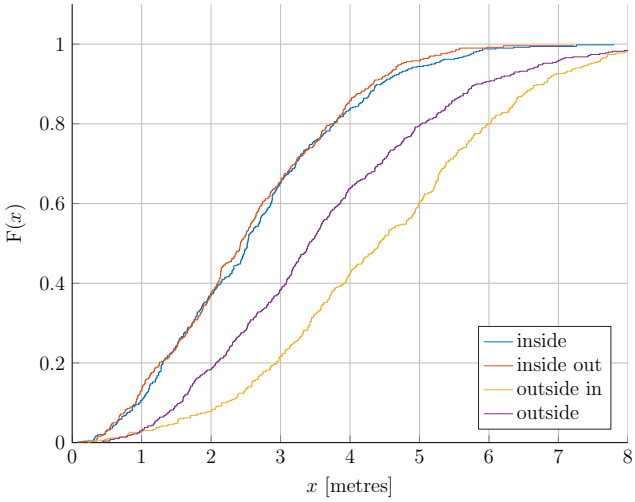

Figure A.4: CDF for FMUg on final points $\sigma = 5, F = 10$.

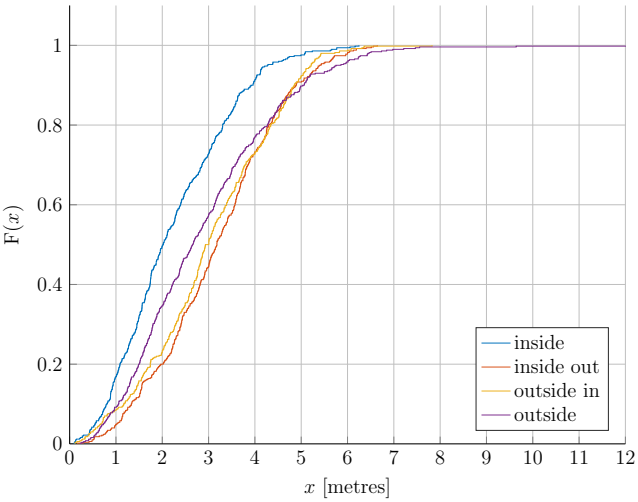

Figure A.5: Simulation B. CDF for FMUg on mid point, $\sigma = 10$.

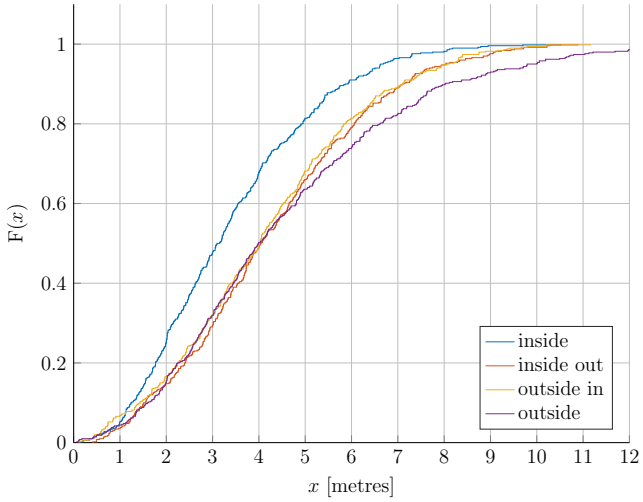

Figure A.6: Simulation B. CDF for FMUg on final point, $\sigma = 10$.

A.2 RMS error

This section presents figures of root mean square of velocity modulus vs. position errors on mid and final point, obtained with our resolution routine using various noise variables during computer simulations. Four area cases are superimposed on each figure.

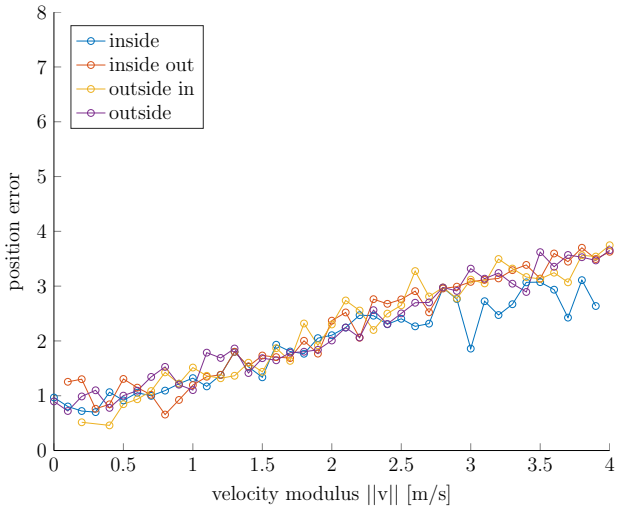

Figure A.7: Velocity modulus vs. position error, 90th percentile on mid point $\sigma = 5$.

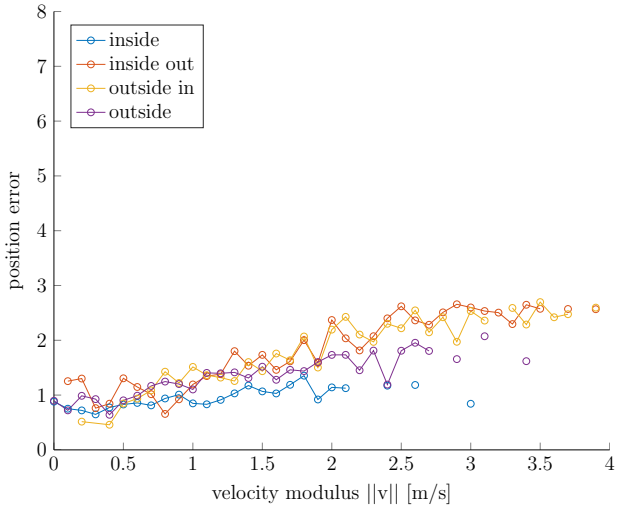

Figure A.8: Velocity modulus vs. position error, median on mid point $\sigma = 5$.

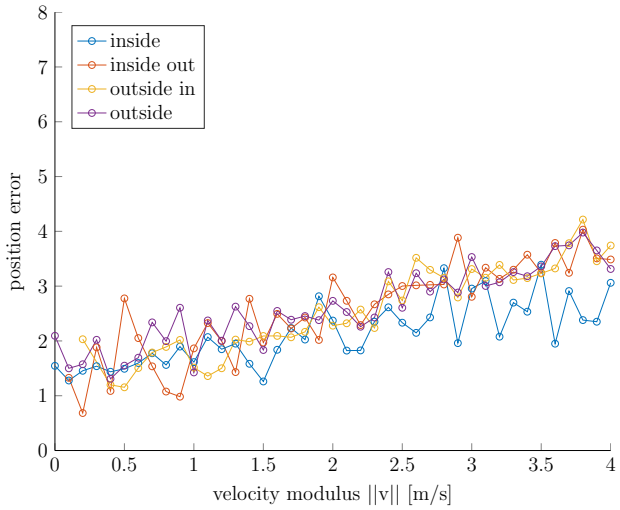

Figure A.9: Velocity modulus vs. position error, 90th percentile on final point $\sigma = 5$.

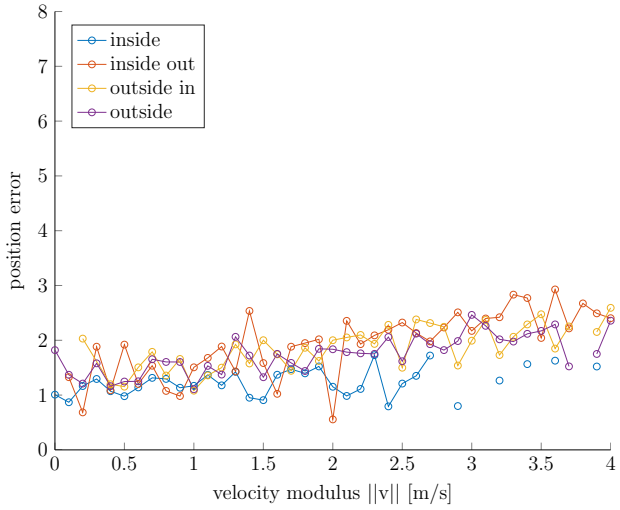

Figure A.10: Velocity modulus vs. position error, median on final point $\sigma = 5$.

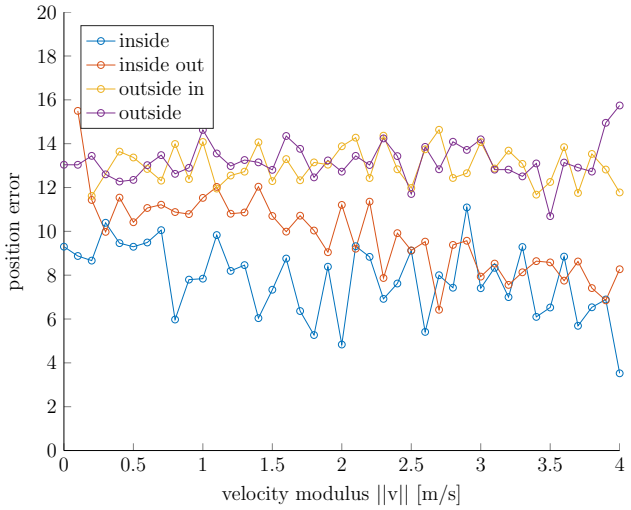

Figure A.11: Velocity modulus vs. position error, RMS on mid point $\sigma = 5, \alpha = 0.5, \beta = 0.5$.

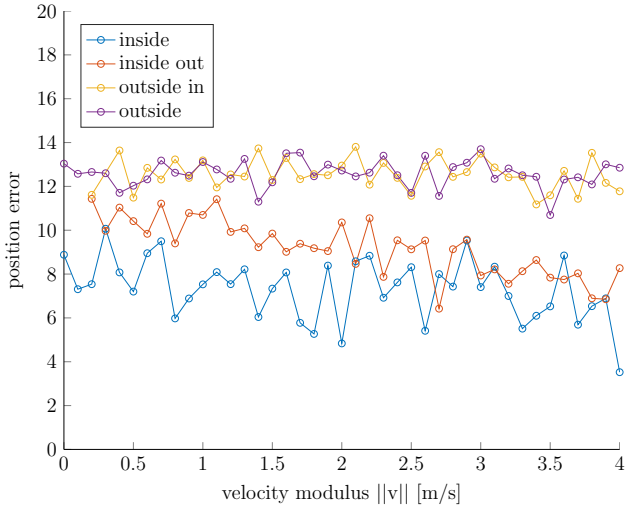

Figure A.12: Velocity modulus vs. position error, 90th percentile on mid point $\sigma = 5, \alpha = 0.5, \beta = 0.5$.

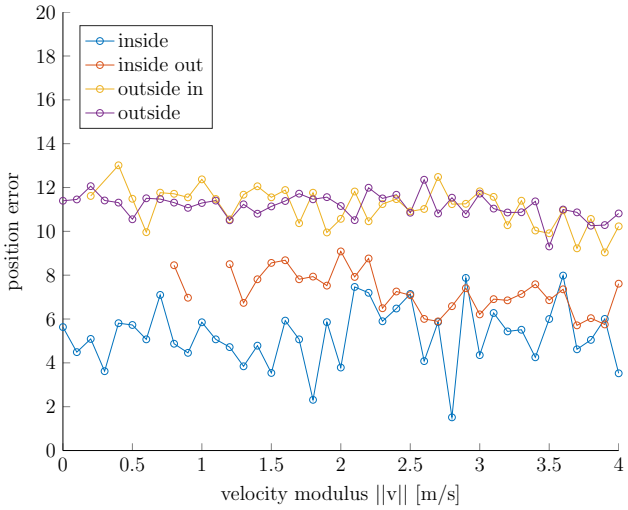

Figure A.13: Velocity modulus vs. position error, median on mid point $\sigma = 5, \alpha = 0.5, \beta = 0.5$.

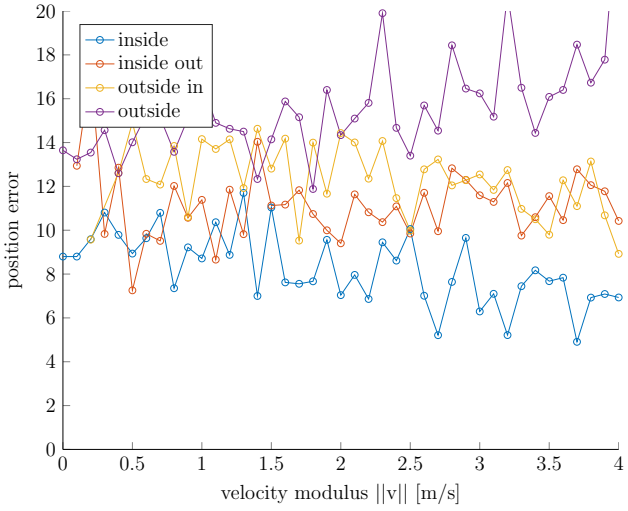

Figure A.14: Velocity modulus vs. position error, RMS on final point $\sigma = 5, \alpha = 0.5, \beta = 0.5$.

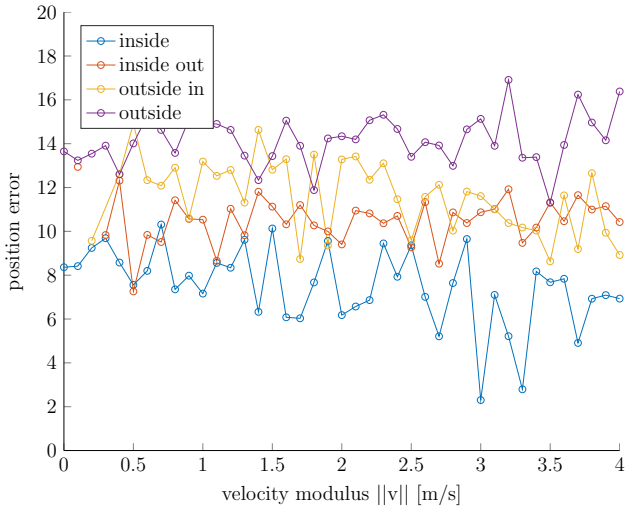

Figure A.15: Velocity modulus vs. position error, 90th percentile on final point $\sigma = 5, \alpha = 0.5, \beta = 0.5$.

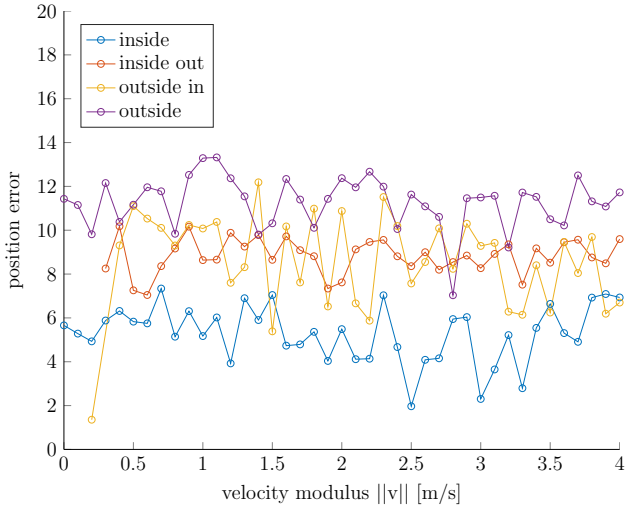

Figure A.16: Velocity modulus vs. position error, median on final point $\sigma = 5, \alpha = 0.5, \beta = 0.5$.

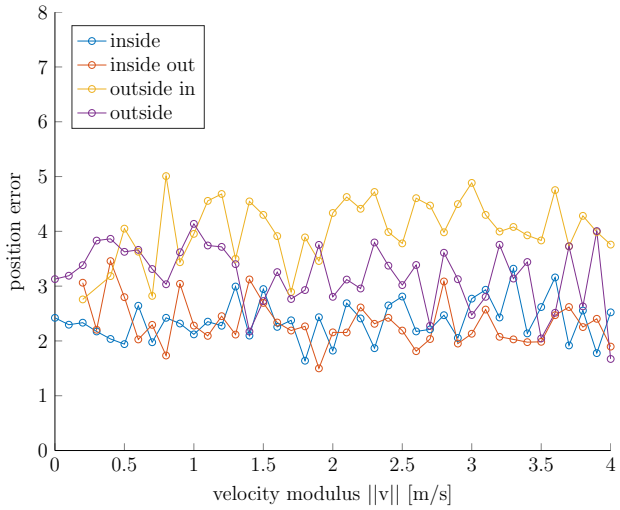

Figure A.17: Velocity modulus vs. position error, 90th percentile on final point $\sigma = 5, F = 10$.

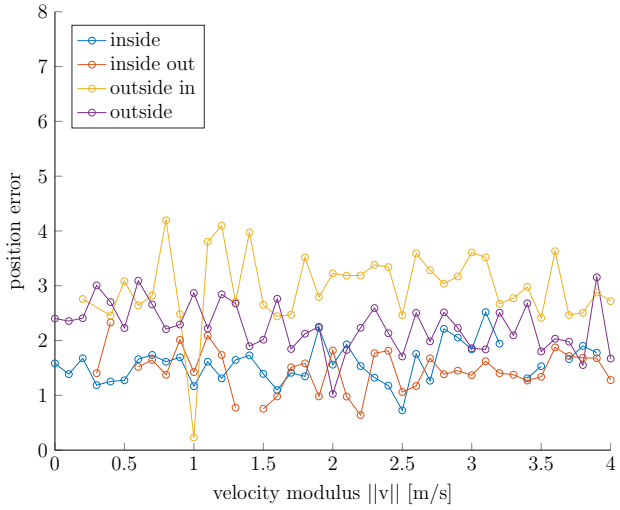

Figure A.18: Velocity modulus vs. position error, median on final point $\sigma = 5, F = 10$.

Appendix B

Garden

B.1 Stationary points

Stationary position estimations for the four experiments performed outdoors in the garden with the lawn mower. Results from all three pruning heuristics are shown in the figures below.

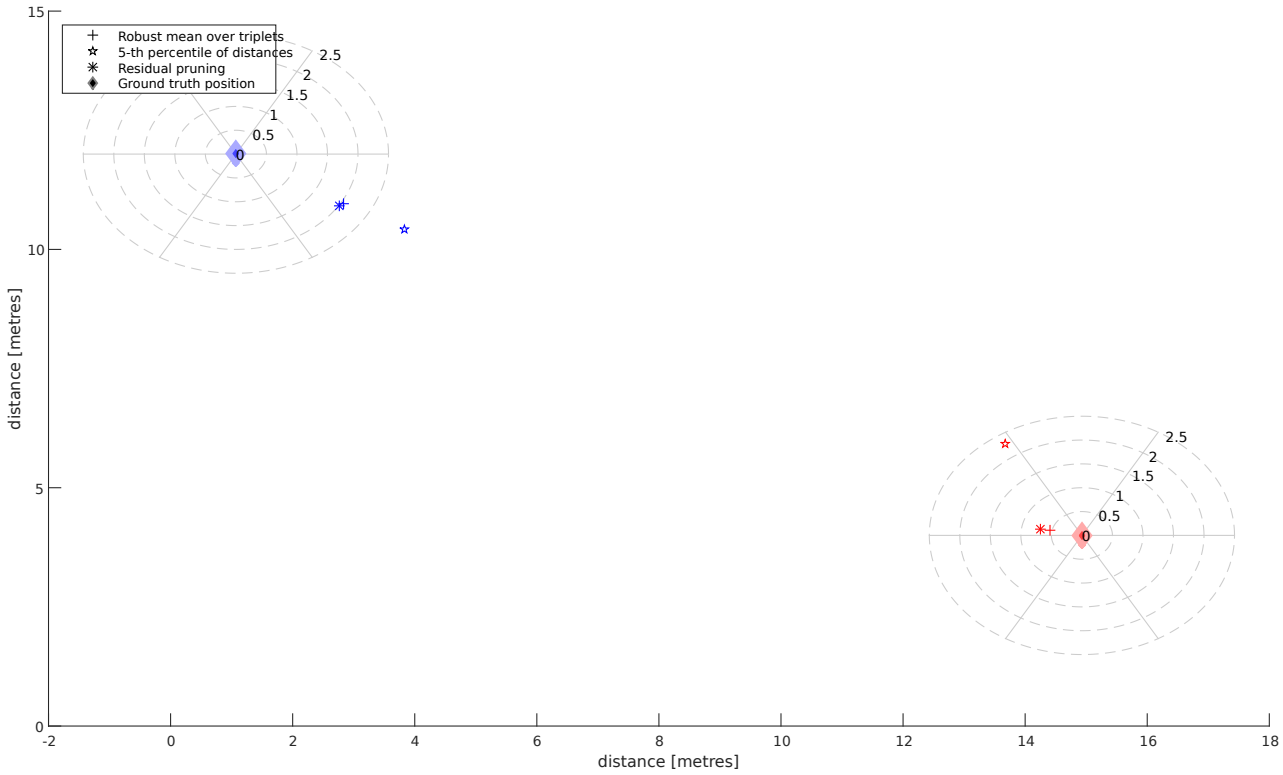

Figure B.1: Static position estimation for the L node (height: 0.45m) — Experiment 2 (fast pace). Residual pruning retention rate: 90%, robust mean with 50% retention rate.

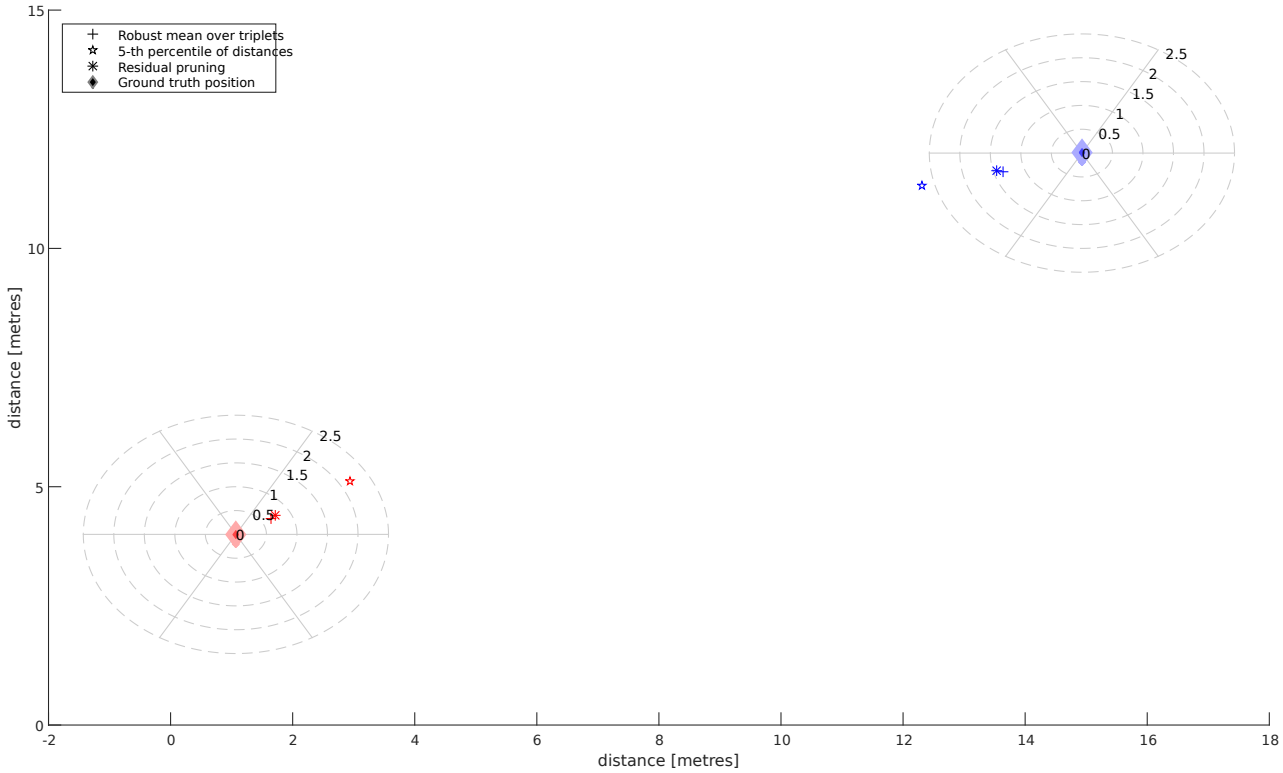

Figure B.2: Static position estimation for the L node (height: 0.45m) — Experiment 3 (slow pace). Residual pruning retention rate: 90%, robust mean with 50% retention rate.

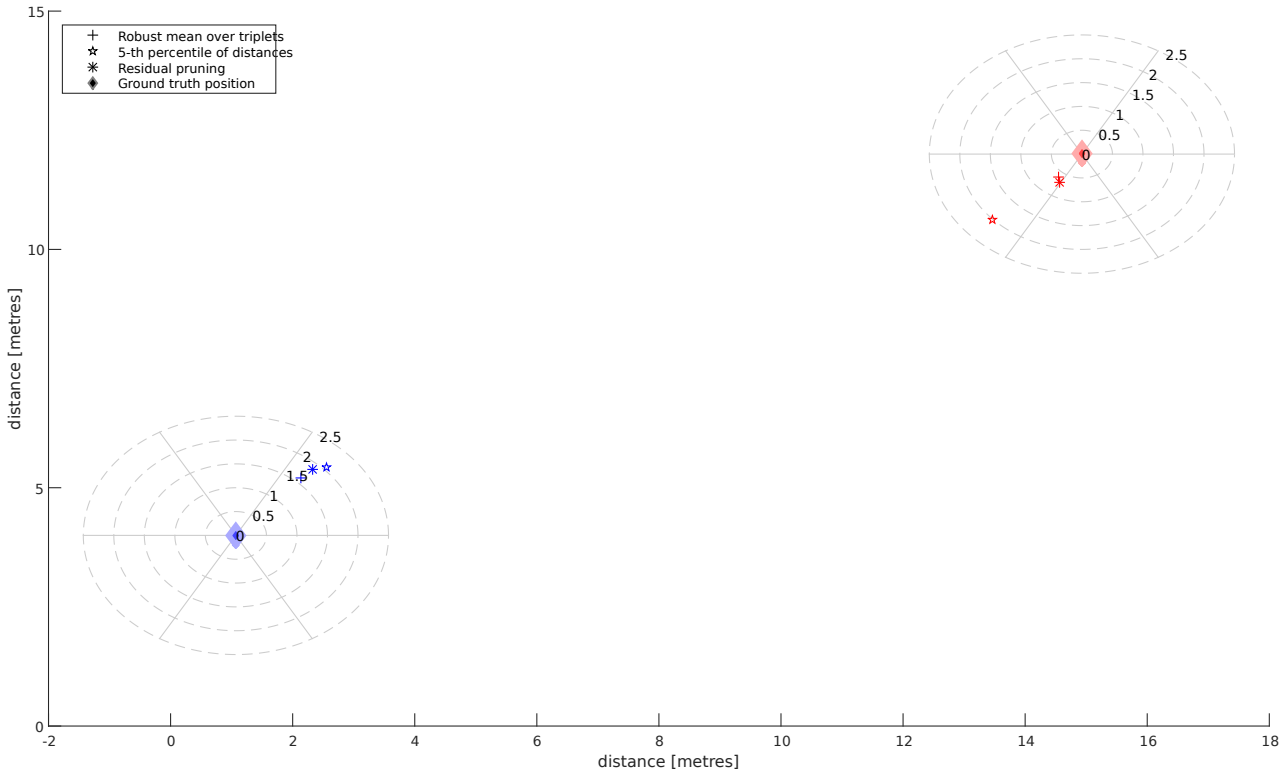

Figure B.3: Static position estimation for the L node (height: 0.45m) — Experiment 4 (fast pace). Residual pruning retention rate: 90%, robust mean with 50% retention rate.

B.2 Trajectories

Trajectory estimations for four outdoor experiments.

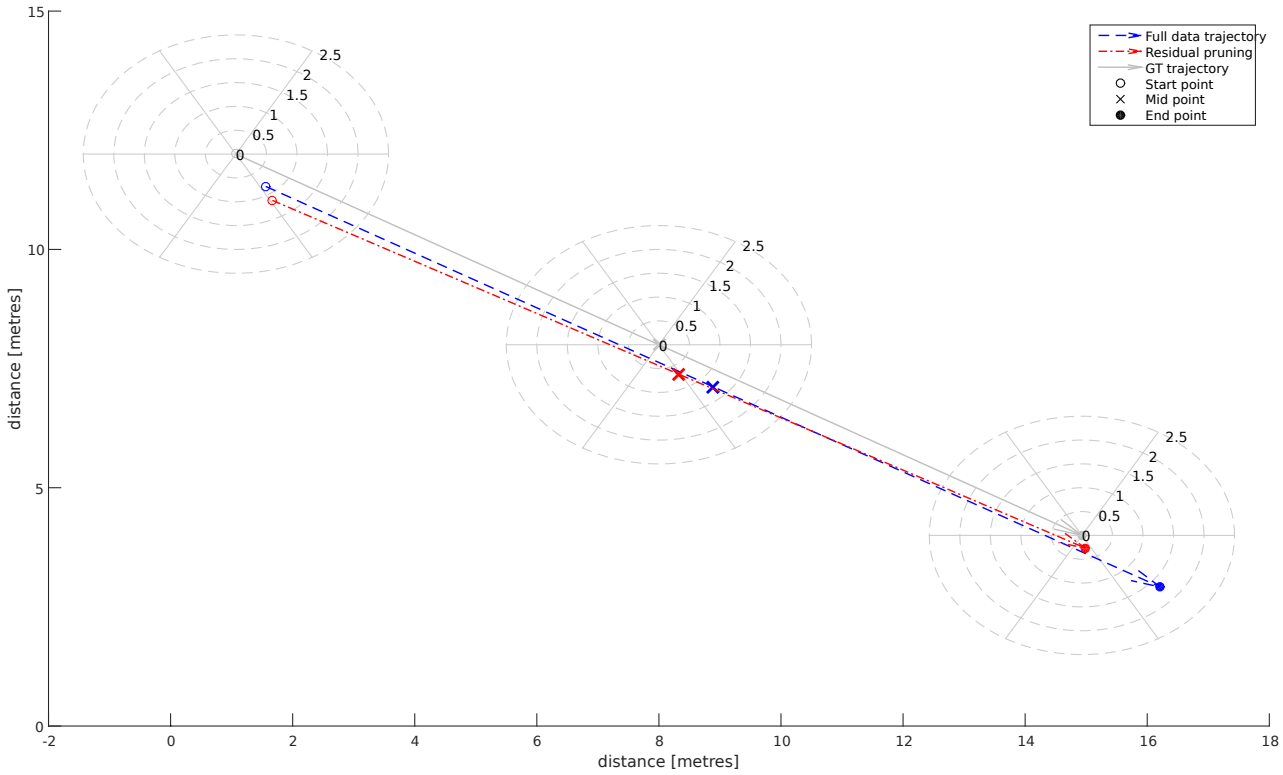

Figure B.4: Trajectory estimation for the L node (height: 0.45m) — Experiment 2 (fast pace). Residual pruning retention rate: 90%.

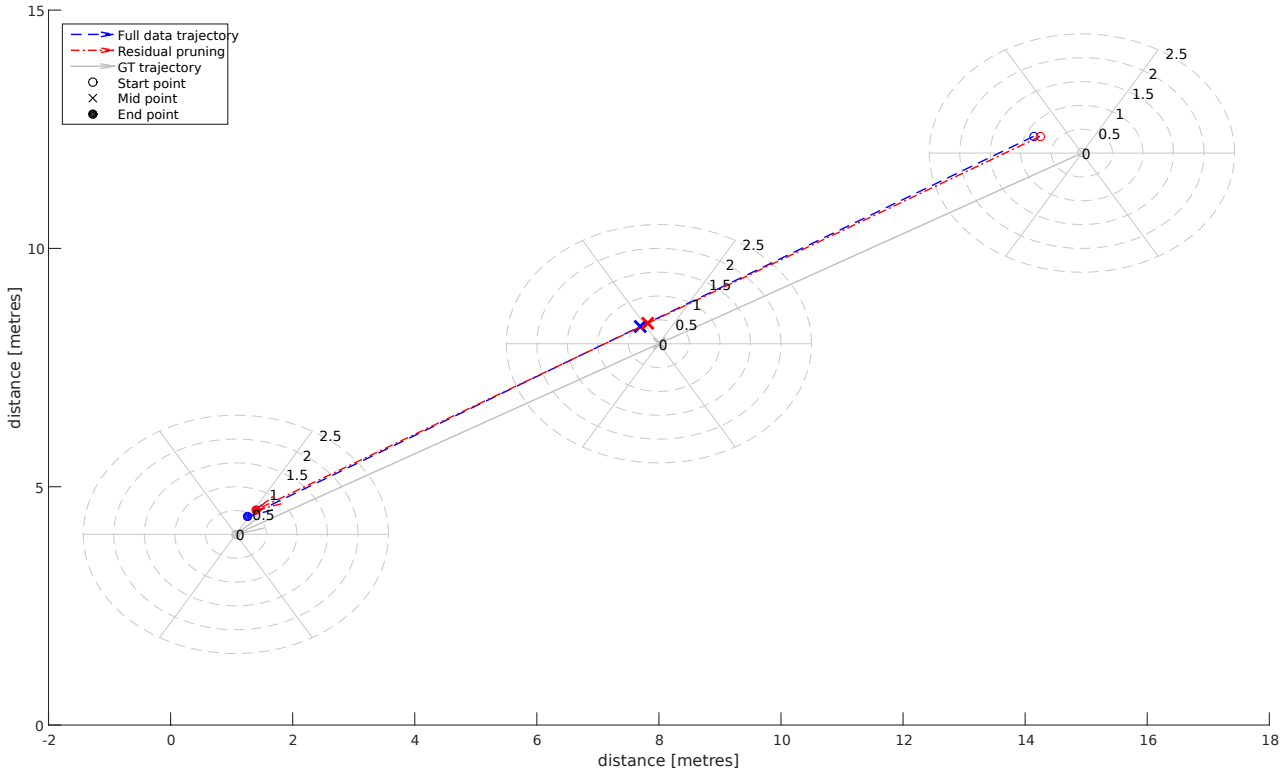

Figure B.5: Trajectory estimation for the L node (height: 0.45m) — Experiment 3 (slow pace). Residual pruning retention rate: 90%.

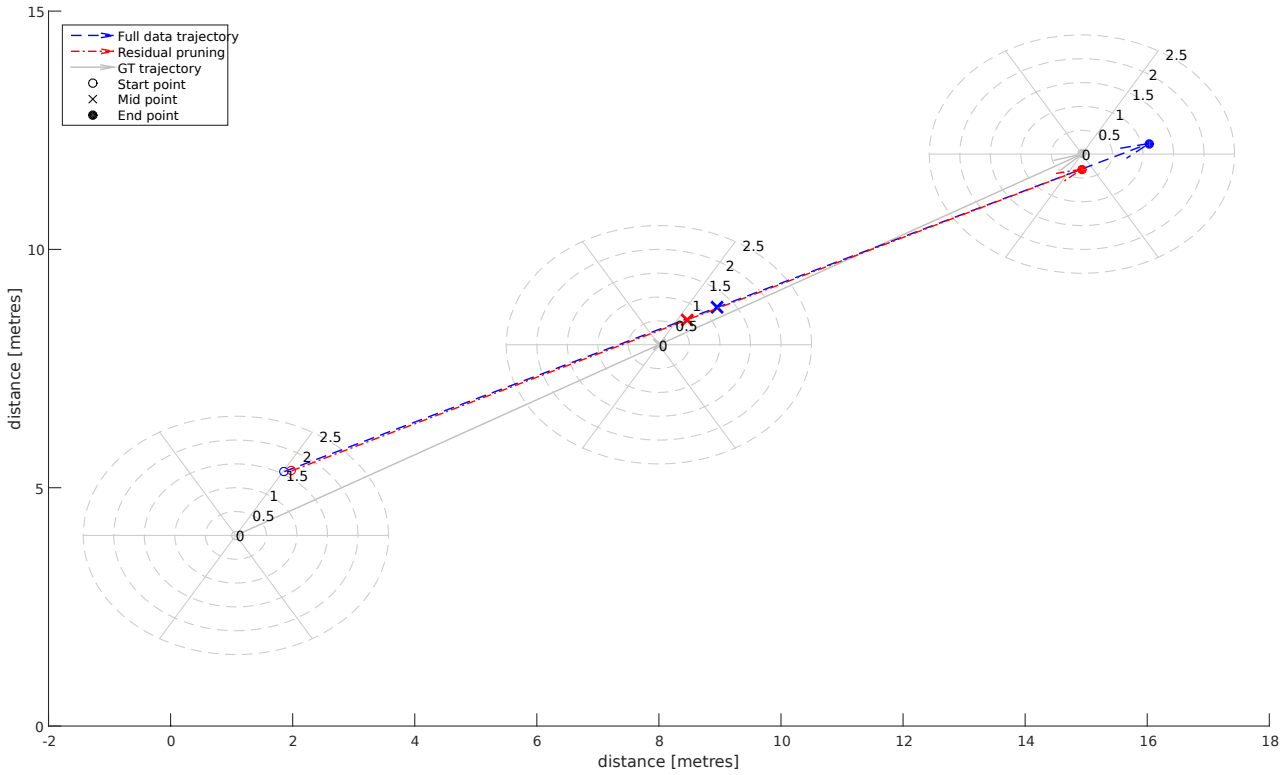

Figure B.6: Trajectory estimation for the L node (height: 0.45m) — Experiment 4 (fast pace). Residual pruning retention rate: 90%.

Appendix C

Dining room

C.1 Stationary points

Stationary position estimations for the six experiments performed indoors in the faculty cafeteria with the IV pole. Results from all three pruning heuristics are shown in the figures below.

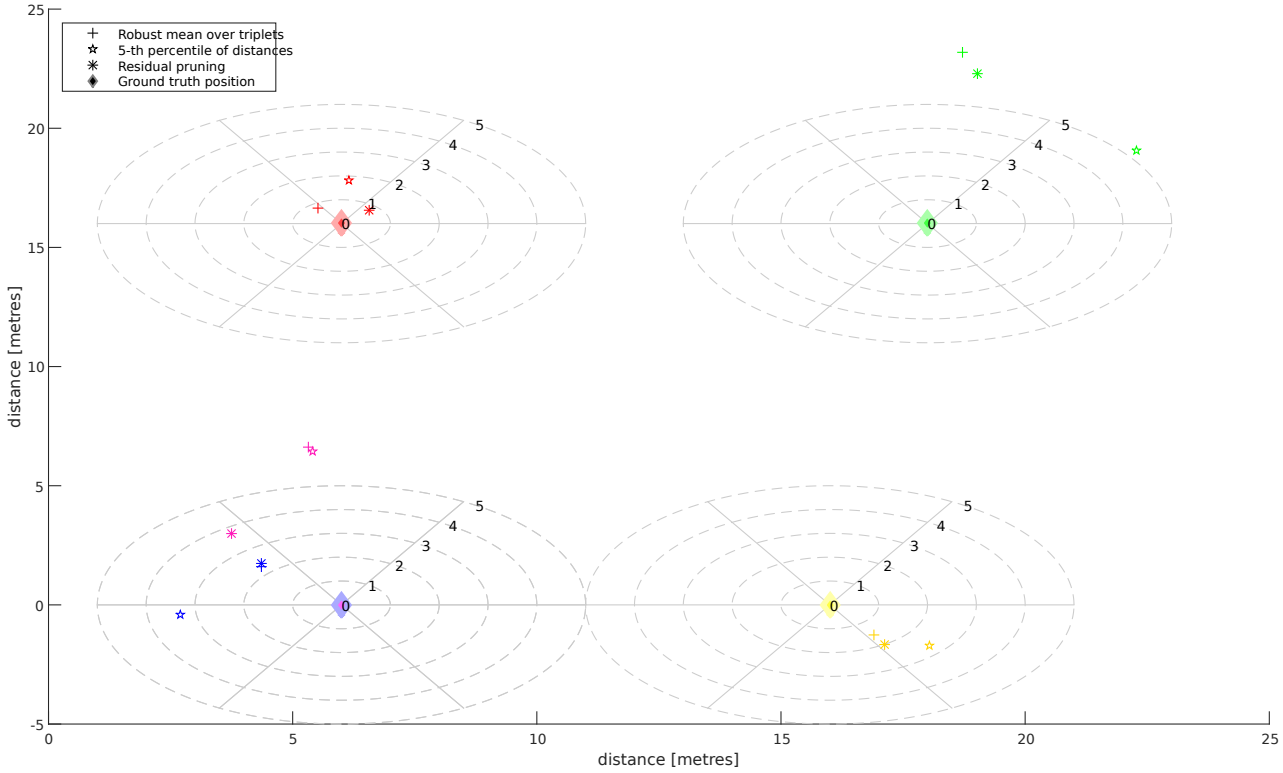

Figure C.1: Static position estimation for the H node at height: 2m — Experiment: 1 (slow pace).

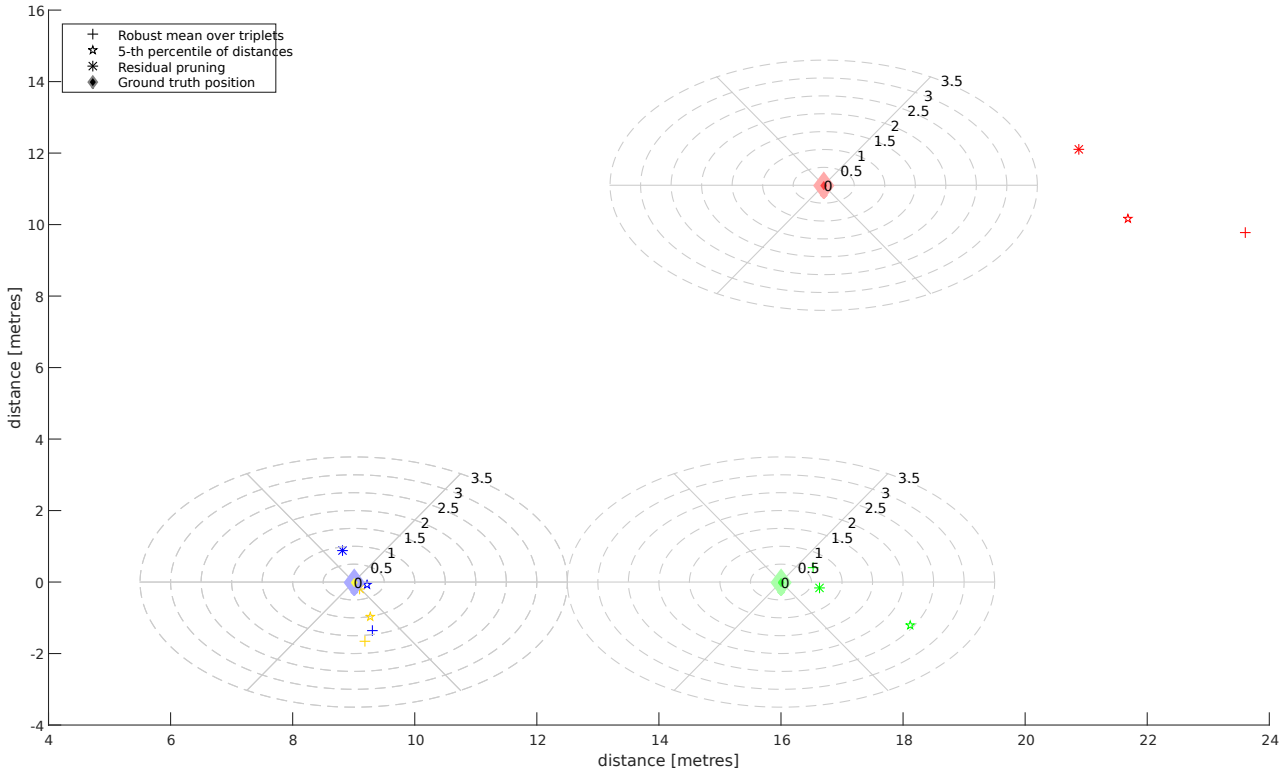

Figure C.2: Static position estimation for the H node at height: 2m — Experiment: 3 (slow pace).

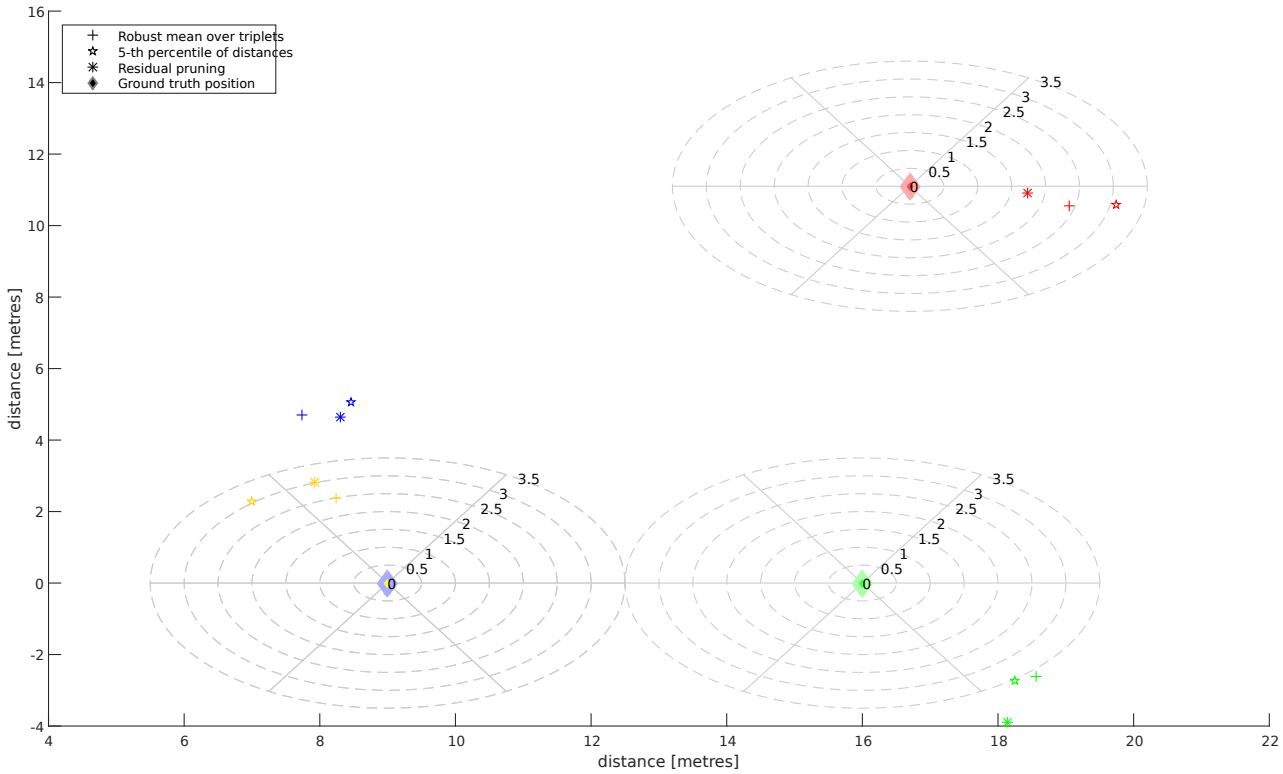

Figure C.3: Static position estimation for the H node at height: 2m — Experiment: 4 (fast pace).

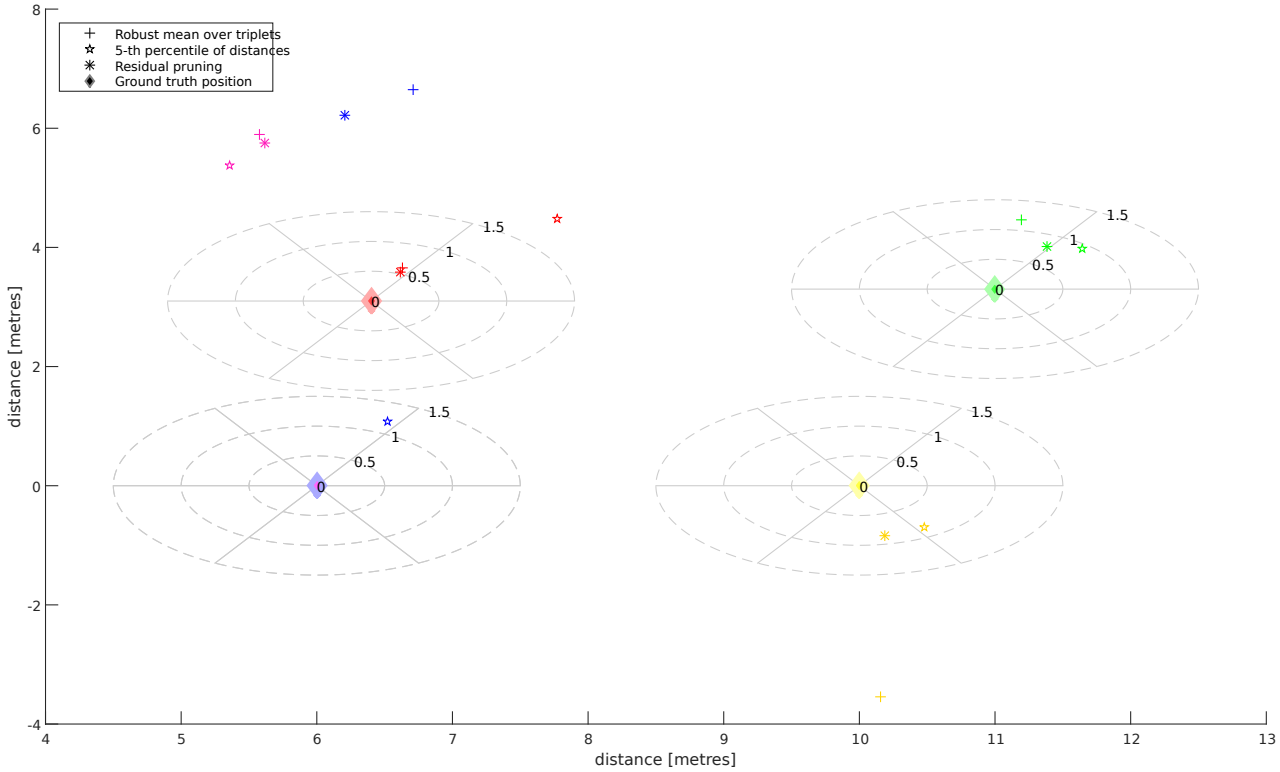

Figure C.4: Static position estimation for the H node at height: 2m — Experiment: 5 (slow pace).

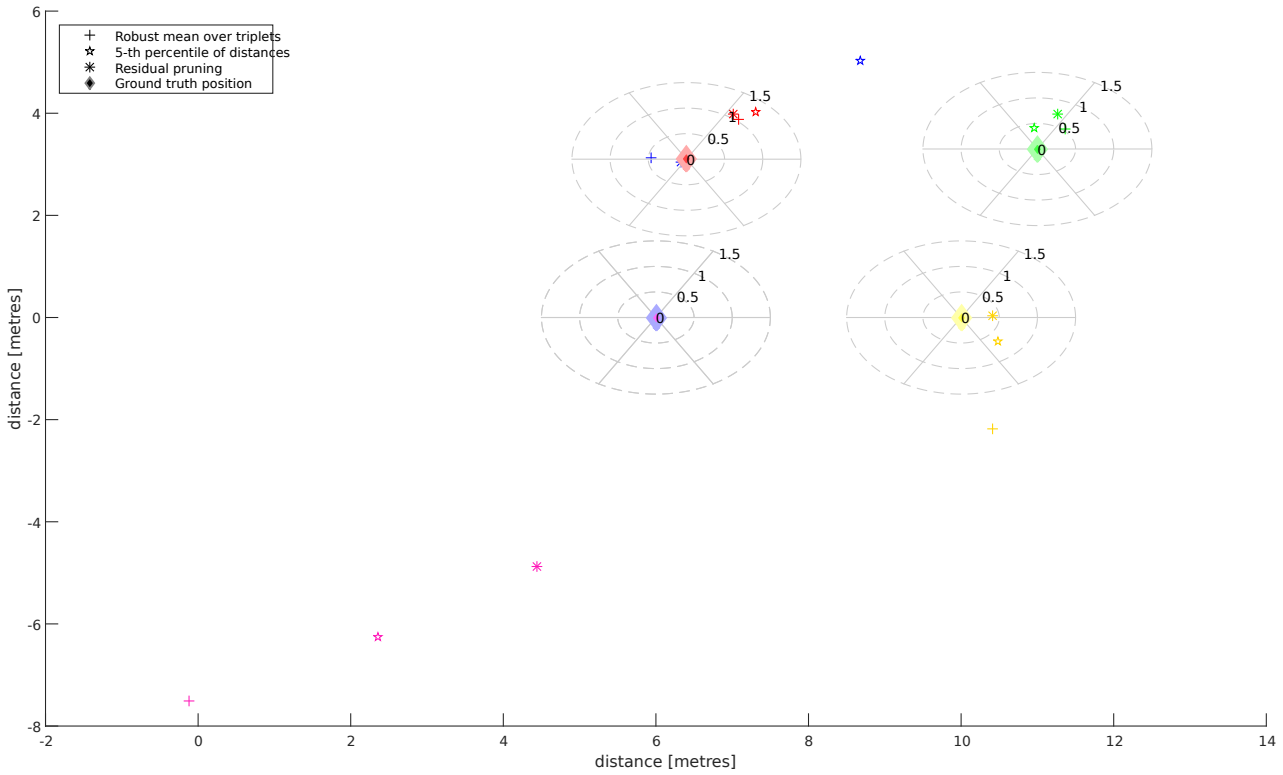

Figure C.5: Static position estimation for the H node at height: 2m — Experiment: 6 (fast pace).

C.2 Trajectories

Trajectory estimations for six indoor experiments.

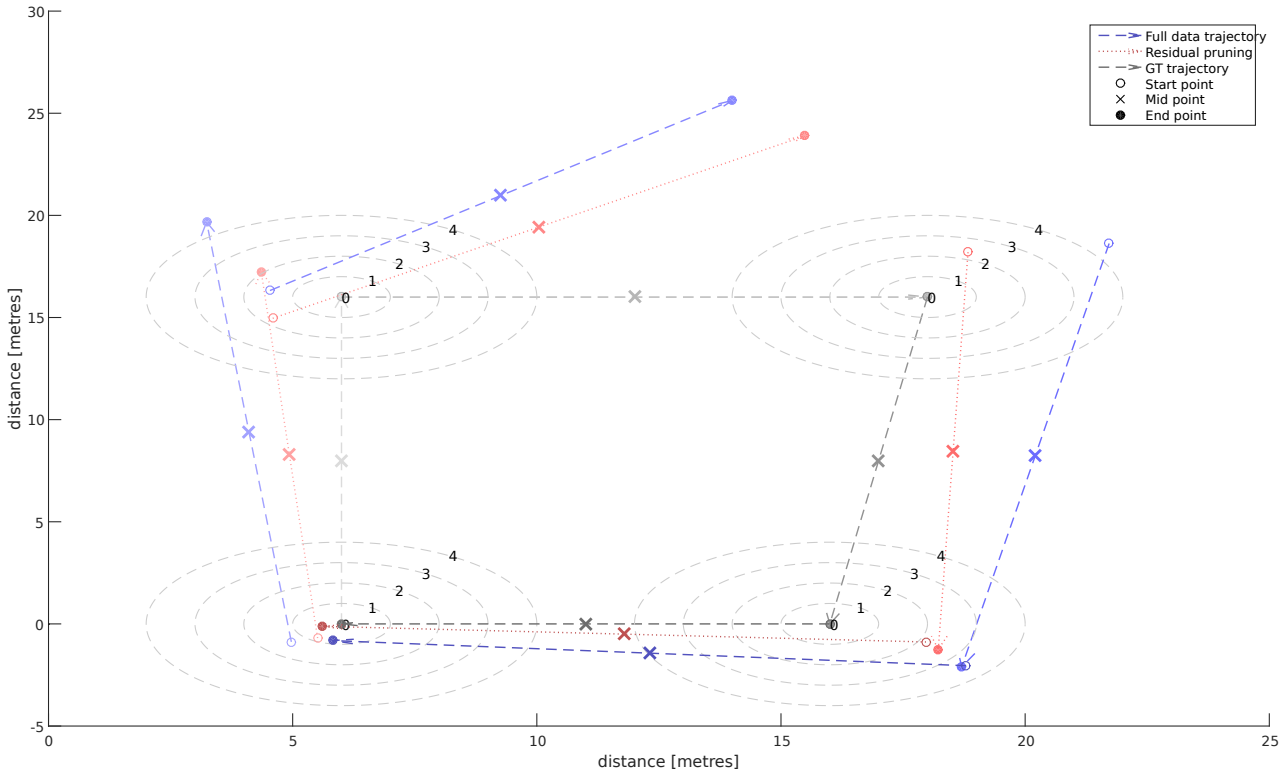

Figure C.6: Experiment 1 (slow pace) trajectories with the H node (height: 2m). Residual pruning retention rate: 90%. Opacity indicates course of the experiment, trajectories fade with time.

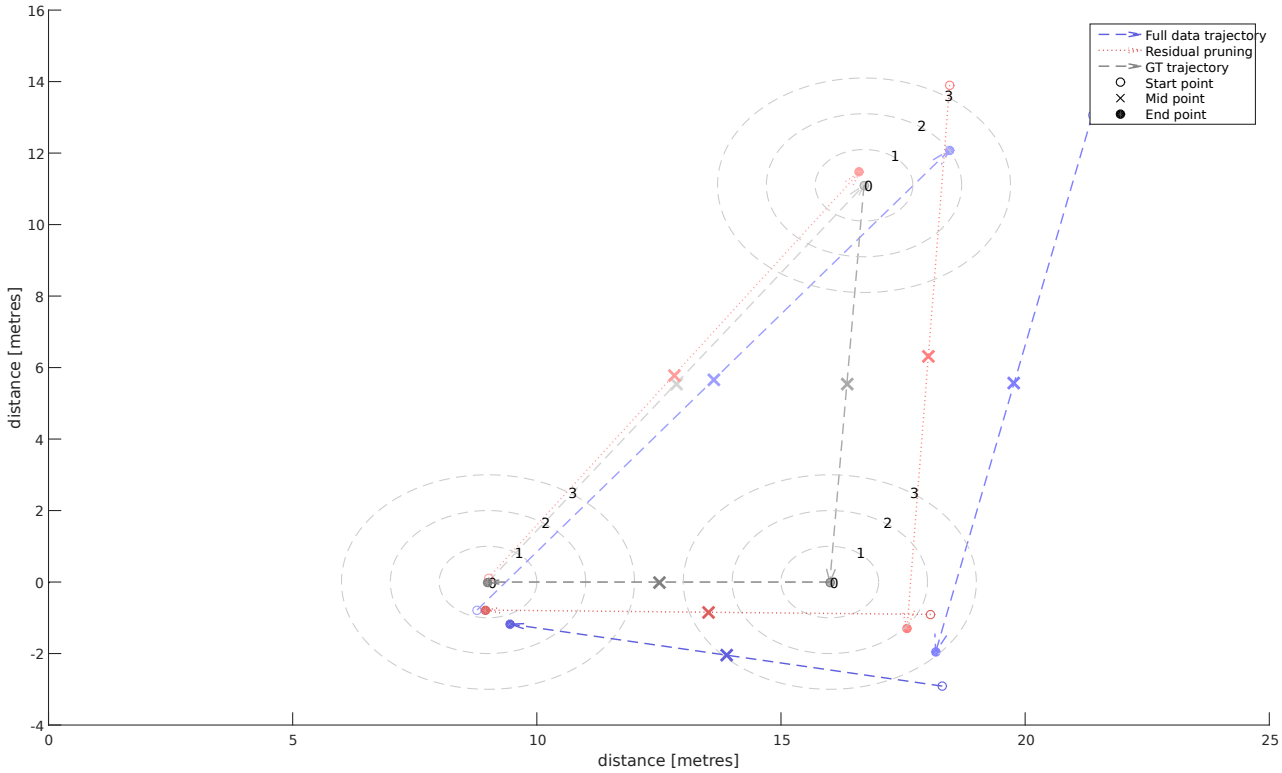

Figure C.7: Experiment 3 (slow pace) trajectories with the H node (height: 2m). Residual pruning retention rate: 90%. Opacity indicates course of the experiment, trajectories fade with time.

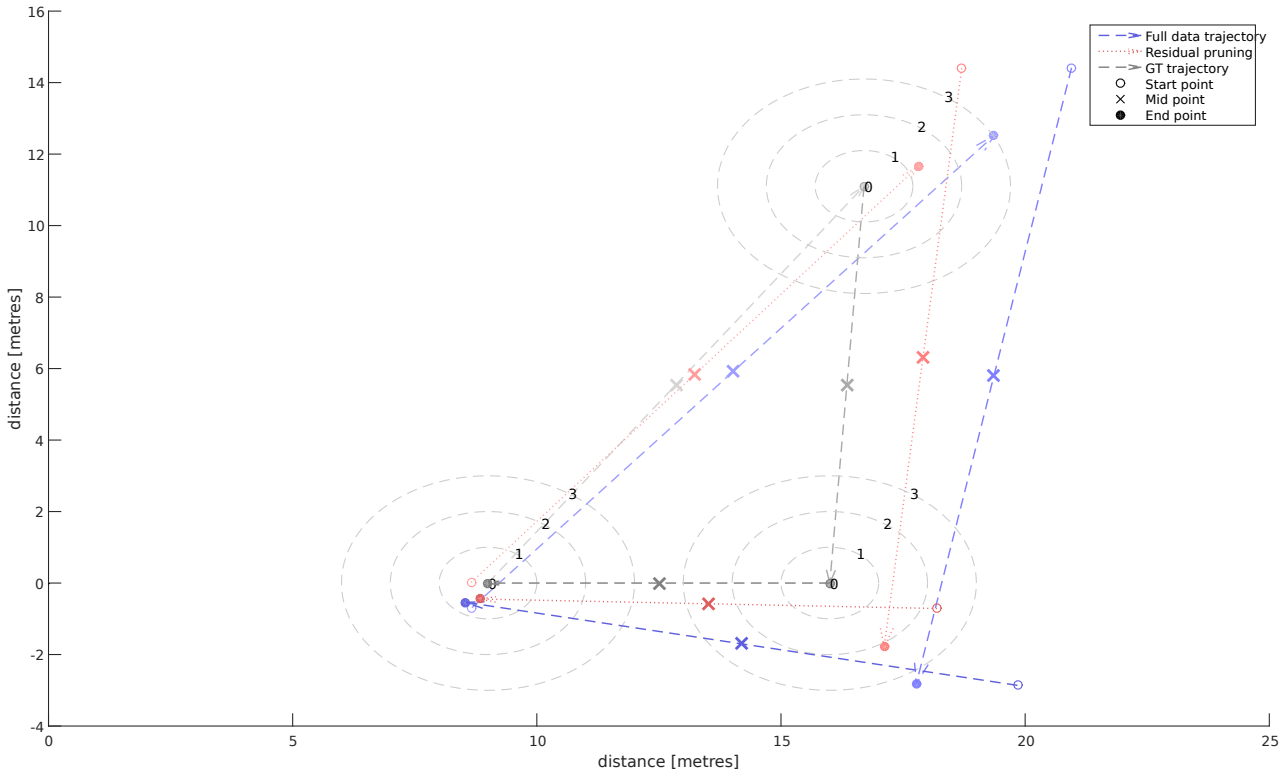

Figure C.8: Experiment 4 (fast pace) trajectories with the H node (height: 2m). Residual pruning retention rate: 90%. Opacity indicates course of the experiment, trajectories fade with time.

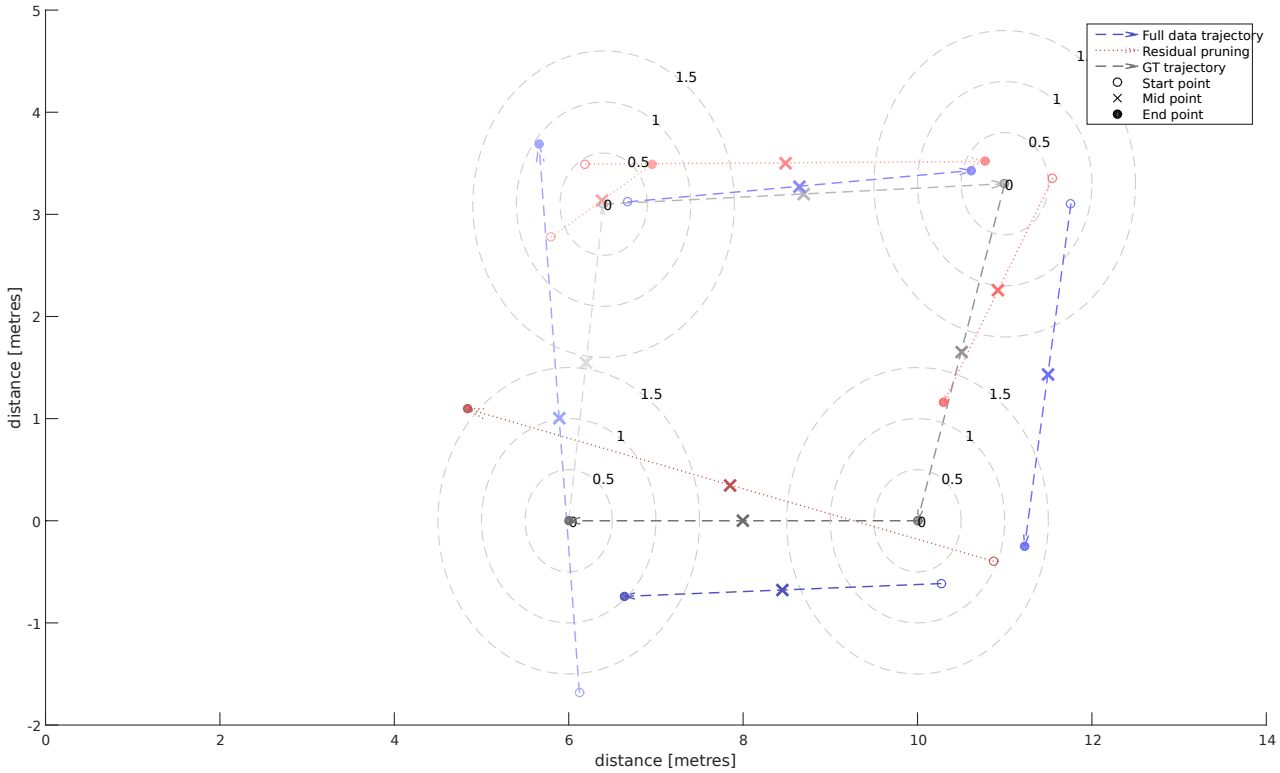

Figure C.9: Experiment 5 (slow pace) trajectories with the H node (height: 2m). Residual pruning retention rate: 90%. Opacity indicates course of the experiment, trajectories fade with time.

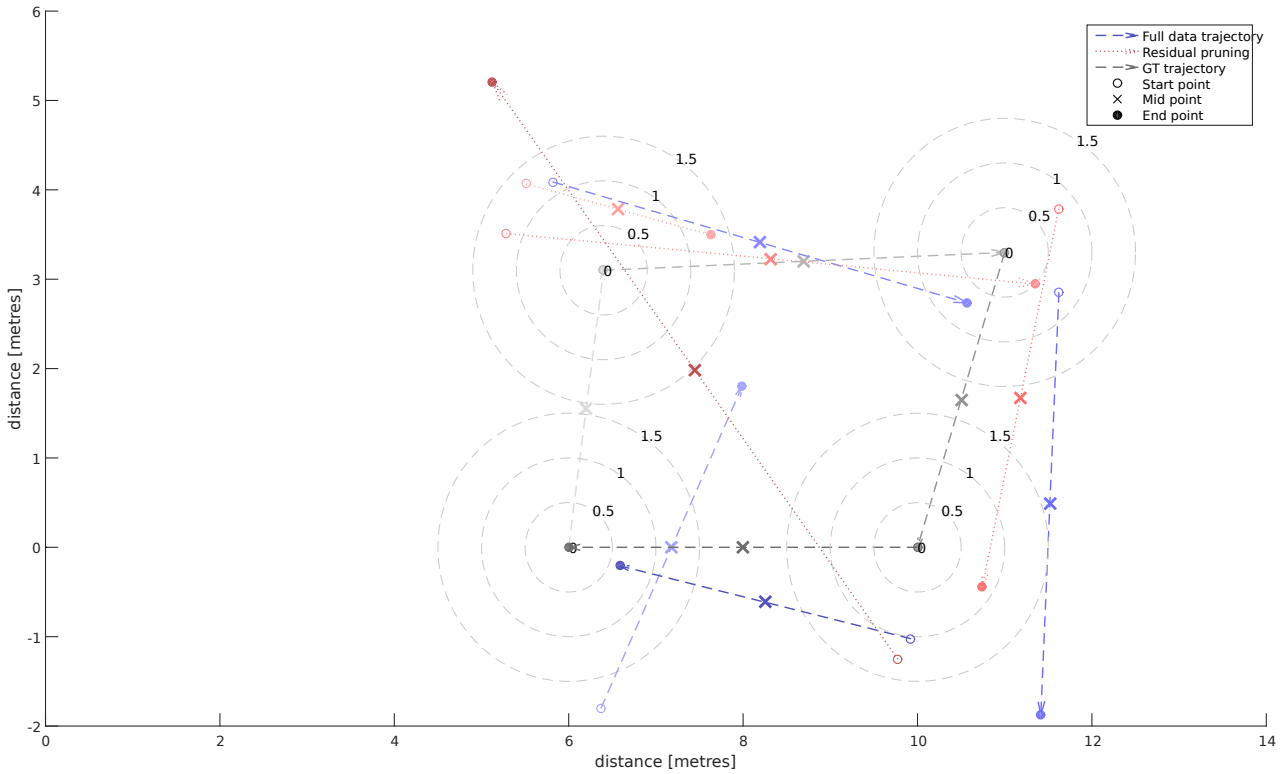

Figure C.10: Experiment 6 (fast pace) trajectories with the H node (height: 2m). Residual pruning retention rate: 90%. Opacity indicates course of the experiment, trajectories fade with time.